International Journal of Machine Tools & Manufacture 198 (2024) 104151

Contents lists available at ScienceDirect

International Journal of Machine Tools and Manufacture

journal homepage: www.elsevier.com/locate/ijmactool

Research Article

Development of a universal, machine tool independent dynamometer for accurate cutting force estimation in milling

G. Totis *, D. Bortoluzzi, M. Sortino

Polytechnic Department of Engineering and Architecture, Università degli Studi di Udine, Via delle Scienze 206, 33100 Udine, Italy

ARTICLE INFO

Keywords:
Milling
Cutting forces
Dynamometer
Filter
Accelerometers
Noise attenuation

ABSTRACT

When integrating a dynamometer into a machining system, it is necessary to identify the dynamic relationship between the effective input forces and the measured output signals (i.e., its transmissibility) through dedicated experimental modal analysis. Subsequently, a filter can be derived and applied to reconstruct the effective input forces from the measured signals. Unfortunately this identification phase can be complex, posing challenges to the device's applicability in both laboratory and industrial conditions. Here this challenge is addressed by introducing a novel dynamometer concept based on both load cells and accelerometers, along with a Universal Inverse Filter. Notably, this filter is independent of the dynamic behavior of the mechanical system where the device is installed. A single calibration suffices, ideally conducted by the device manufacturer or by an expert, allowing the dynamometer's integration by a non-expert user into any machining system without the need for repeating the identification phase and the filter generation. Furthermore, this new concept offers another significant advantage: it attenuates all inertial disturbances affecting the measured signals, including those arising from the cutting process and those originating from exogenous sources such as spindle rotation, linear axes' movements, and other vibrations propagating through the machine tool structure. To illustrate, a simplified model is introduced initially, followed by an overview of the novel dynamometer design, innovative identification phase, and filter construction algorithm. The outstanding performance of the novel (non-parametric) Universal Inverse Filter – about 5 kHz of usable frequency bandwidth along direct directions and 4.5 kHz along cross dir. – was experimentally assessed through modal analysis and actual cutting tests, compared against state of the art filters. The efficacy of the new filter, which is even simpler than its predecessors, was successfully demonstrated for both commercial and taylor-made dynamometers, thus showing its great versatility.

1. Introduction

Estimating the effective cutting forces exchanged between the cutting tool and the workpiece during a machining operation plays a crucial role for studying cutting process mechanics and dynamics [1], for the development of innovative cutting tools with complex geometries [2], and for solving problems with materials having a low machinability.

In addition, instantaneous cutting force estimation may enable advanced process monitoring and diagnosis [3,4], optimization [5] and even real-time control of the cutting process [6,7].

Detecting the quasi-static forces may be sufficient for some basic tasks, such as the detection of tool wear during repetitive machining operations. In some cases, quasi-static cutting forces and cutting torque can be derived from the servo-control units governing the main spindle and the linear axes of a CNC machine [8] or the robotic joints of a robotic milling system [9]. However, it must be noticed that the inner signals of the servo-control units (such as torque, velocity, tracking error) are rarely available – especially at a sufficiently high sampling frequency – to the final user. Alternatively, quasi-static forces can be estimated by using relatively cheap external sensors, provided that they are sufficiently sensitive to the cutting forces under interest.

Nevertheless, an accurate estimation of rapidly time-varying cutting forces may be necessary for more advanced tasks, such as for tool design optimization, tool breakage detection and for real-time control of the cutting process.

In the last decades, the research on new devices and methodologies for cutting force estimation has pursued the following goals:

1. improving the primary sensing elements and the inner structure of the device to extend the usable frequency bandwidth without

* Corresponding author.
E-mail address: giovanni.totis@uniud.it (G. Totis).

https://doi.org/10.1016/j.ijmachtools.2024.104151
Received 27 February 2024; Received in revised form 19 March 2024; Accepted 21 March 2024
Available online 26 March 2024

Nomenclature

$\mathbf{F}_{inp}$	Effective input forces applied to workpiece
$\mathbf{F}_{ext}$	External forces which are not applied to the workpiece
$\mathbf{S}_{dyn}$	Measured load cells' signals
$\mathbf{A}_{base}$	Measured accelerations of dynamometer base
$\mathbf{T}(j\omega)$	Transmissibility of the dynamometer installed at a given setup
$\mathbf{T}_{\infty}(j\omega)$	Transmissibility of the dynamometer under infinitely stiff clamping conditions
$\mathbf{H}(j\omega)$	Transmissibility between accelerations of dynamometer base and the measured load cells' signals
$\mathbf{G}(j\omega)$	Transfer function between the external/exogenous forces and the dynamometer base accelerations
$\mathbf{L}(j\omega)$	Transfer function between the input forces applied to the workpiece and the dynamometer base accelerations
$\mathbf{B}(j\omega)$	Transfer function between the measured load cells' signals and the input forces
$\mathbf{C}(j\omega)$	Transfer function between the dynamometer base accelerations and the input forces
F_i	Generic input force applied to the workpiece at a given position, along a given dir.
R_w	Component of the global cutting force along the wth direction
N	Length of each signals' transient acquired during the pulse tests
Q	Number of the available dynamometer outputs
Q'	Number of the available acceleration signals
P	Number of the distinct input force positions
B_{wr}	Frequency bandwidth associated to wr directions
R_{ww}	Squared linear correlation coefficient between filtered and simulated forces along direction w
D	External cutter diameter
Z_t	Number of teeth
n	Spindle speed
f_z	Feed per tooth
a_p	Axial depth of cut
a_L	Lateral width of cut
$a_{L,1}$	Lateral distance between cutter barycenter and the edge of the workpiece where the cutting edge enters
γ_n	Normal rake angle
γ_a	Axial rake angle
r_ε	Nose radius
χ	Cutting edge angle
$dF_{c,j}$	Infinitesimal main cutting force at a given point of tooth j
$dF_{r,j}$	Infinitesimal radial cutting force at a given point of tooth j
$dF_{a,j}$	Infinitesimal axial cutting force at a given point of tooth j
dA_j	Infinitesimal uncut chip section area associated to an element of cutting edge j
$k_{w,q}$	S&P cutting force model coefficients, where $w = c, r, a$ and $q = s, p$

TFRF	Transmissibility Frequency Response Function
OIF	Optimal Inverse Filter
SOIF	Superior Optimal Inverse Filter
URDF	Upgraded Regularized Deconvolution Filter
UIF	Universal Inverse Filter (new developed here)

applying any filter (at least none more advanced than a simple low-pass filter);
2. inventing effective filters capable of reconstructing the three-dimensional input cutting forces in a wide frequency range, for a given experimental setup where the device is embedded;
3. extending the frequency bandwidth of both the direct and cross transmissibilities through the filter application;
4. getting rid of the identification phase (mathematical interpolation of experimental modal analysis data) required by parametric filters, by developing better non-parametric filters, which are numerically derived from the non-parametric modal analysis data;
5. solving the dependence of dynamometer transmissibilities from the input force position, for a given force direction;
6. eliminating the need of repeating the modal analysis phase each time the device is mounted on a new experimental setup.
7. filtering both endogenous (caused by the cutting process) and exogenous (caused by other external sources) inertial disturbances affecting the dynamometer signals.

The last two goals were never tried, but successfully achieved here.

It is worth noting that all the developed parametric and non-parametric filters require to perform modal analysis each time the device is mounted on a given machining system, which is typically a complex task done by skilled operators. Can we eliminate this phase by providing a kind of universal filter, which is valid for all machining systems independently from their dynamic behavior? Does a universal filter exist, which is capable of compensating for any dynamometer transmissibility?

Surprisingly, the answer is positive, as it will be shown in this work. This breakthrough result can be obtained by estimating the translational and rotational accelerations of dynamometer base by means of dedicated accelerometers, and then by reconstructing the input forces from the combination of force and acceleration signals, through the new, non-parametric Universal Inverse Filter (UIF) conceived here. This filter is the result of an innovative, non-trivial modal analysis procedure which will be explained in the next sections.

2. State of the art about dynamometers and filtering techniques for advanced milling applications

Piezoelectric dynamometers represent the best solution for cutting force measurement in milling since they are very stiff, sensitive and characterized by a good signal to noise ratio even in micromilling operations, where the forces are less than 1 N [10,11]. One possible disadvantage of piezoelectric sensing devices is their insensitiveness to static force terms. However, in milling we are interested in quasi-static and dynamic forces. The former can be determined with good accuracy by setting to zero the signals when the tool is outside the workpiece. In the following the removal of any quasi-static offset or drift from the signals will be taken for granted. Additionally, it has to be recalled that piezoelectric devices are quite expensive and often incompatible with process automation. Thus, their application is generally limited to R&D activities.

For advanced milling applications – such as those performed with relatively small cutting tool diameters rotating at high spindle speeds – a wide frequency bandwidth is required to accurately characterize the

most important harmonics composing the dynamic cutting forces. The actual limit of the best devices – when they are installed into actual machining systems – is about $0.1 \div 2.5$ kHz, depending on the details of the mechanical configuration [12]. This is generally not sufficient for an in-depth characterization of cutting process dynamics.

One reason for such dynamic behavior is the presence of inertial mass in front of the sensing elements, which converts vibration into undesired inertial disturbances. Additionally, this behavior is influenced by the dynamic properties of the machine tool substructure where the device is integrated [13]. For example, a platform dynamometer is significantly impacted by the inevitable vibration modes of the machine tool table – dynamometer – workpiece subsystem [14]. Conversely, a rotating dynamometer [15–17] is strongly influenced by the dynamic compliance of the spindle housing – spindle – tooling subsystem. This influence can be mitigated by minimizing the mass in front of the sensor through the use of lightweight and sensitive sensors. This was done by Luo et al. [18], who embedded thin PVDF sensors between each cutting insert and the cutter body. However, this issue becomes more pronounced when dealing with flexible machining systems such as robotic arms [19], which are commonly utilized for milling large structures in the aerospace sector.

Structural modifications of the measuring device are not sufficient to improve its dynamic characteristics, and the only possibility to extend the usable frequency bandwidth consists in the application of advanced signal processing techniques.

For this purpose, many solutions have been devised in the last 20 years, with an increasing level of complexity and effectiveness.

The first successful attempts have been one-dimensional (only one single direction was corrected) by using an Augmented Kalman Filter [10,20]. A full and effective 3D approach was hindered for many years by the complex dynamics of the platform dynamometer, which cannot be simply described by a 3×3 transmissibility matrix.

In detail, the classic 3×3 transmissibility matrix model inadequately captures the dependence on input force position, in addition to its direction. To address this limitation, an expanded dynamic model with more inputs and outputs was introduced to enable full 3D correction. This approach, known as the Upgraded Augmented Kalman Filter [21], surpasses the former AKF in terms of accuracy and effectiveness. However, it remains parametric, relying on a mathematical model that must be identified after the experimental modal analysis phase using sophisticated techniques. This crucial step demands the expertise of a skilled professional, making it potentially unsuitable for industrial applications.

Therefore, more efforts have been recently devoted to development of non-parametric approaches, which overcome the problem of model identification. Experimental modal analysis for measuring dynamometer transmissibilities is still necessary, but then all the signals are elaborated through a non-parametric, numerical procedure, thus practically eliminating the need of human intervention for filter construction.

With this aim, the Upgraded Regularized Deconvolution Filter (URDF) was conceived in [12], which was based on the expanded dynamic model of dynamometer transmissibility introduced in [21] and on the application of regularization techniques for a robust inversion of the large, ill-conditioned matrix representing the dynamic relation between system inputs and outputs [22,23], whence the filter is eventually obtained. This approach is an extension of a technique proposed in [24], which was practically limited to the direct directions, i.e. by neglecting the cross-talk disturbances. This improved technique was also based on the fundamental works of Qiao et al. [25,26].

Nevertheless, URDF is feasible only when the system is characterized by Finite Impulse Responses (FIRs) having a short time duration. When slender parts are attached above the measuring device, their long-lasting free oscillations imply very long and colored FIRs, which cannot be easily inverted through the URDF algorithm. For this purpose, the Superior Optimal Inverse Filter (SOIF) was eventually introduced, which operates in the frequency domain [14]. This is a non-trivial extension of the former Optimal Inverse Filter that was initially proposed by Castro et al. in 2006 [27], and then further refined by other authors [28–30].

In short, according to the results of modal analysis and cutting tests reported in [14], the SOIF is the most effective non-parametric solution available at the moment for suppressing undesired signal fluctuations caused by inertial disturbances.

However, all the former filters do strongly rely on the preliminary modal analysis phase, which is necessary to determine the effective transmissibility of the device when it is embedded into a given experimental setup. In the perspective of industrial applications, it is desirable to eliminate this phase. This result was achieved here by proposing a new device architecture – including both load cells and accelerometers – and by computing a kind of universal filter, which is suitable for any generic experimental setup independently from its dynamics. However, the construction of such universal filter (which will be called Universal Inverse Filter — UIF) will require a special modal analysis (executed only once), as it will be explained in the next sections.

It is worth noting that the use of accelerometers in combination with load cells have been already proposed in technical literature, but not for this specific task.

In 1995, Spiewak attempted to estimate cutting forces solely from spindle accelerations measured by a triaxial accelerometer integrated into the rotating toolholder, yielding promising results up to approximately 1 kHz [31].

A few years later, Tounsi et al. [32] developed a correction method for a platform dynamometer in the frequency domain. They achieved this by estimating the acceleration of the dynamometer-workpiece barycenter using seven monoaxial accelerometers strategically positioned above the platform. Their results demonstrated effective compensation of dynamometer transmissibilities up to 2 kHz in both direct and cross directions. However, this study did not explore the dependence of dynamometer dynamics on input force location, and the achieved frequency bandwidth after compensation remained limited for modern applications that require higher spindle speeds. This pioneering work was brilliant and very promising, yet it relied on a classic modal analysis procedure for transmissibility measurement and filter construction, which was inadequate to generate a universal filter. In practice, no exogenous training was conducted by exciting the dynamometer base instead of the workpiece mounted on top of it. As demonstrated here, this classic approach falls short when the device is mounted on a new experimental setup, unless the modal analysis is repeated in such configuration and the filter is recalculated. Additionally, this approach proves ineffective for canceling exogenous inertial disturbances.

Afterwards, Chae et al. attached an accelerometer to the workpiece in a micromilling application for a better correction of dynamometer dynamics [10]. Acceleration and force signals were both given as inputs to an Augmented Kalman Filter (AKF), thus attaining a good real-time correction up to about 4.5 kHz. Nevertheless, the proposed approach was still one-dimensional, and both cross-talk errors and exogenous noise were not taken into account.

In a recent work [33] accelerometers were installed at the spindle housing, and their data, along with spindle current signals, were utilized for real-time force monitoring without the need for other invasive sensors, such as piezoelectric dynamometers. Current signals were exploited to estimate the static components of cutting forces, while acceleration signals were employed for estimating their dynamic components using the Kalman observer approach. Although these results were satisfactory for industrial applications at low spindle speeds, they are not sufficient for most advanced high-speed milling operations, since the achievable bandwidth was less than 1 kHz.

Postel et al. in [34] achieved a better outcome by extending the usable bandwidth to 1.6 kHz through the use of multiple accelerometers attached to the spindle housing at different positions. However, reliable

estimation of static force terms remained elusive as additional signals sensitive to these terms were not included.

Alternatively, Takahei et al. in 2022 [35] utilized servo-control signals of the linear axis moving the machine tool table, in combination with an accelerometer attached to the workpiece fixture, to reconstruct cutting forces and indirectly estimate cutting force model coefficients and modal parameters of the machining system. This approach, assisted by the accelerometer, proved equivalent to using a dynamometer for estimating cutting forces up to approximately 0.6 kHz.

Recently, force reconstruction was obtained in robotic milling using accelerometers located on the spindle housing and a capacitive force sensor between the end effector and the spindle housing [36]. Again, the AKF approach was adopted. Since the final transmissibility of the device strongly depends on the peculiar robot configuration owing to the pose-dependent dynamics of robotic arms [37], the system was also trained by using a machine-learning-based identification algorithm. After training, this method was capable of recognizing the dominant vibrations modes of the structure for any generic configuration, in order to correct their effects on the estimated cutting forces. However, it is worth noting that the Kalman observer is a parametric method, and its ability to suppress exogenous noise remains unclear.

A further evidence that cutting forces can be accurately derived from acceleration signals is presented in [38]. However, reconstructing the quasi-static components solely from accelerometers is challenging due to their poor signal-to-noise ratio in the low-frequency range. In [38] the (parametric) Kalman filter was compared to a non-parametric technique based on regularized deconvolution, showing the advantages and limitations of both methods, with the Kalman approach proving more effective in the low-frequency domain.

Recently, the conjugate gradient least square method was applied in the time domain for force reconstruction from acceleration signals in peripheral milling [39], showcasing another non-parametric method that simplifies the preliminary identification phase drastically.

However, none of the previous research works were focused on the development of a universal, machine tool independent filter, capable of eliminating the need of re-calibration and all kinds of inertial disturbances. The present work aims to bridge this gap by introducing a novel non-parametric device and filter, which has to be calibrated just once by the manufacturer of the device or by an expert user and then directly applied to any machining system by a possibly non-expert user without any further re-calibration. In addition, the proposed system is capable of suppressing both endogenous noise caused by the cutting process and exogenous noise deriving from any external vibration source. Furthermore, this novel method significantly simplifies the filter construction procedure outlined in a previous study [14], thus facilitating its prospective implementation in real-world industrial applications.

3. Working principles of the universal dynamometer by means of a simplified model

In order to explain the behavior of a generic dynamometer when it is embedded into a machine tool let us consider the scheme of Fig. 1.

During the cutting process, the effective input cutting force F_{inp} is exchanged between the cutting tool and the workpiece, thus causing deformations and vibrations propagating throughout the entire machining system, both from the side of tool and from the side of workpiece, thus possibly perturbing the measured forces in different ways. Let us assume that the dynamometer senses the measured force F_{dyn}, which is in general different from F_{inp}. Dynamometer transmissibility can be defined as

$$T(j\omega) = \frac{F_{dyn}(j\omega)}{F_{inp}(j\omega)} \tag{1}$$

According to the adopted simplified model illustrated in Fig. 1, it is easy to show that

$$F_{dyn}(j\omega) \cong k_2\left(u_2 - u_1\right) + c_2\left(\dot{u}_2 - \dot{u}_1\right) \tag{2}$$

Thus, the force measured by dynamometer is strictly related to the degrees of freedom u_1 and u_2 and on their velocities, which will depend on the cutting force $F_2 = F_{inp}$ applied to the workpiece, on the reaction force $F_3 = -F_{inp}$ applied to the cutting tool and to other unknown external forces F_0, F_1 and F_4 applied to machine tool structure.

When the machine tool basement is assumed infinitely stiff the reaction force $F_3 = -F_{inp}$ acting on the tool has no significant effects on F_{dyn}. In addition, no further (known) disturbances are generally considered in the analysis, i.e. F_1, F_0 and F_4 are typically neglected. Nevertheless, this is not true in general. By relaxing these oversimplifications, it is clear that unwanted noise may affect the dynamometer signals due to the reaction cutting force and to the unknown external sources of vibrations. The latter are caused by motors and kinematic chains which are responsible for mechanical power transmission inducing axes movements and spindle rotation. In addition, further disturbances may come from other parts of the machine tool, such as its auxiliaries. Other noise may be also generated by the machining operations executed on other components, as occurring in a transfer machine.

Thus, in general we should write

$$F_{dyn} = F_{dyn}\left(F_{inp}, \mathbf{F}_{ext}\right) \tag{3}$$

where $\mathbf{F}_{ext}$ is a vector including all the external forces. Thus, input force reconstruction is difficult because $\mathbf{F}_{ext}$ is unknown as well as the transfer function from $\mathbf{F}_{ext}$ to F_{dyn}.

However, all the dynamic effects caused by the external disturbances $\mathbf{F}_{ext}$ are incorporated into the vibration u_1, together with the effects caused by F_{inp} according to the linear superposition principle. Thus, the knowledge of such vibration could effectively substitute the lack of information regarding $\mathbf{F}_{ext}$. For this purpose, the acceleration a_1 of the node 1 can be measured by applying an accelerometer.

In short, dynamometer transmissibility can be expressed as a function of F_{inp} and a_1 alone, the latter being considered as a given, known input instead of a causal output. For this purpose, let us start from the dynamic equilibrium equation of mass m_2, that is

$$m_2\ddot{u}_2 = -k_2\left(u_2 - u_1\right) - c_2\left(\dot{u}_2 - \dot{u}_1\right) + F_{inp} \tag{4}$$

where k_2 and c_2 denote the modal stiffness and damping, respectively, of the workpiece-dynamometer subsystem with respect to the remainder of the machining system. This conceptualization involves a cross section of the sensing device at the point where the force is detected. After simple algebra in the Fourier domain one arrives at

$$U_2 = \frac{1}{m_2(j\omega)^2 + c_2 j\omega + k_2} F_{inp} + \frac{k_2 + c_2 j\omega}{\left[m_2(j\omega)^2 + c_2 j\omega + k_2\right]} \frac{A_1}{(j\omega)^2} \tag{5}$$

where U_2 is the Fourier Transform of u_2 and A_1 is the Fourier Transform of the acceleration a_1 of the lumped mass m_1. Thus, U_2 is the dynamic consequence of F_{inp} and A_1.

Let us now focus on the measured force, which can be expressed by

$$F_{dyn} = \left(k_2 + c_2 j\omega\right)\left(U_2 - \frac{A_1}{(j\omega)^2}\right) \tag{6}$$

which can be finally rewritten in the following form

$$F_{dyn}(j\omega) = \underbrace{\left[\frac{k_2 + c_2 j\omega}{m_2(j\omega)^2 + c_2 j\omega + k_2}\right]}_{T_\infty(j\omega)} F_{inp}(j\omega) + \underbrace{\left[\frac{\left(k_2 + c_2 j\omega\right)\left(-m_2\right)}{m_2(j\omega)^2 + c_2 j\omega + k_2}\right]}_{H(j\omega)} A_1(j\omega) \tag{7}$$

thus showing the direct, linear dependence of F_{dyn} on F_{inp} and on A_1 alone, without any explicit mention to $\mathbf{F}_{ext}$.

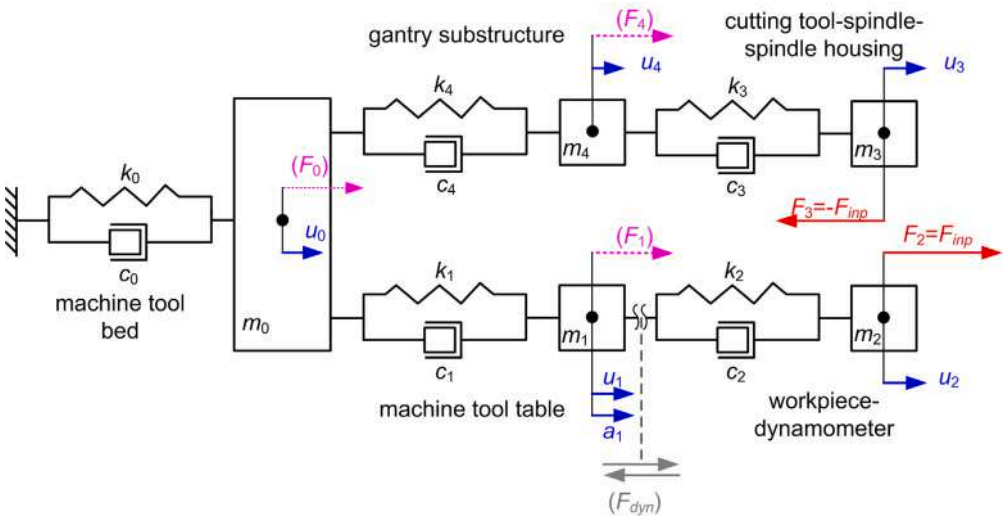

Fig. 1. Simplified model for explaining the principles of accelerometric compensation applied to a dynamometer installed into a CNC machine tool.

By exploiting the linear superposition principle, acceleration A_1 can be expressed as the sum

$$A_1(j\omega) = L(j\omega)\,F_{inp}(j\omega) + \delta A_1(j\omega) \tag{8}$$

where $L(j\omega)$ is the transfer function representing the effects of the input force applied to the workpiece when all the other forces are set to zero, whereas the second term is the perturbation induced by the reaction force applied to the tool $-F_{inp}$ and by the all the external disturbances $\mathbf{F}_{ext}$, when the force applied to the workpiece is set to zero.

By substituting Eq. (8) into Eq. (7) it yields

$$F_{dyn}(j\omega) = \underbrace{\left[T_\infty(j\omega) + H(j\omega)\,L(j\omega)\right]}_{T(j\omega)} F_{inp}(j\omega) + H(j\omega)\,\delta A_1(j\omega) \tag{9}$$

where $T(j\omega)$ is the classic Transmissibility Frequency Response Function (TFRF) defined in Eq. (1), that is the main result of the conventional modal analysis phase. The second contribution is negligible only when the perturbation $\delta A_1(j\omega)$ is very small. Otherwise, it may give a significant contribution that cannot be neglected, as it will be proven later.

It is fundamental to observe that $T_\infty(j\omega)$ and $H(j\omega)$ do not depend on the details of the subsystem behind accelerometer position. On the contrary, $T(j\omega)$ and $\delta A_1(j\omega)$ depend on such details and on the exogenous forces. Nevertheless, since the total acceleration $A_1(j\omega)$ at node 1 (i.e. at dynamometer base position) is available, neither the effective device transmissibility $T(j\omega)$ nor the effects of the exogenous disturbances $\mathbf{F}_{ext}$ must be known for a correct input force reconstruction.

It is now convenient to go back to Eq. (7), which can be rewritten as follows

$$F_{dyn}(j\omega) = \underbrace{\left[T(j\omega) - H(j\omega)\,L(j\omega)\right]}_{T_\infty(j\omega)} F_{inp}(j\omega) + H(j\omega)\,A_1(j\omega) \tag{10}$$

showing the perfect cancellation of the machine tool-dependent term $H(j\omega)L(j\omega)$ from $T(j\omega)$, yielding the machine tool-independent transmissibility $T_\infty(j\omega)$.

In a more general situation we will have

$$\mathbf{S}_{dyn}(j\omega) = \mathbf{T}_\infty(j\omega)\,\mathbf{R}_{inp}(j\omega) + \mathbf{H}(j\omega)\,\mathbf{A}_{base}(j\omega) \tag{11}$$

where $\mathbf{R}_{inp}$ contains the 3 global input force components $R_{inp,x}$, $R_{inp,y}$ and $R_{inp,z}$; $\mathbf{A}_{base}$ are the measured accelerations of dynamometer base thought as a rigid body having 6 degrees of freedom; $\mathbf{T}_\infty$ and $\mathbf{H}$ are the dynamic relations connecting such inputs to the measured dynamometer signals $\mathbf{S}_{dyn}$ (12 in our case), as illustrated in Fig. 2.

During the cutting process the input force is applied at different input locations on the workpiece, thus influencing the final dynamometer dynamics. In the current case it is imagined that such input forces are represented as the global input forces located at workpiece center plus ad hoc additional momenta which introduce a disturbance which will be eliminated by the obtained filter. However, it is very important to excite the workpiece at different locations in order to train the system to implicitly recognize and compensate such disturbances.

In order to estimate the key transmissibilities $\mathbf{T}_\infty(j\omega)$ and $\mathbf{H}(j\omega)$, the following procedure is proposed.

1. The device should be endowed with a sufficient number, type and configuration of accelerometers to estimate the 6 degrees of freedom of dynamometer base.
2. The device is mounted on a very stiff experimental setup; under such conditions, the following transmissibility can be derived:

$$\mathbf{T}_\infty(j\omega) \cong \frac{\mathbf{S}_{dyn}(j\omega)}{\mathbf{R}_{inp}(j\omega)} \tag{12}$$

   In other words, if dynamometer base was mounted on an infinitely stiff machine tool bed, neither the external/exogenous forces nor those acting directly on the workpiece would be capable of moving it. This is mathematically equivalent to

$$\mathbf{G}(j\omega) \approx \mathbf{L}(j\omega) \approx 0 \Rightarrow \mathbf{A}_{base}(j\omega) \approx 0 \tag{13}$$

   which does heuristically prove Eq. (12). However, it is not essential to assure perfectly rigid clamping conditions to achieve the former result. Any industrial machine tool table or any massive industrial table can be adequate for performing the first identification step. The discrepancy between the perfectly rigid clamping conditions and the real clamping conditions will be implicitly and automatically taken into account by the proposed algorithm.
3. Afterwards, the device is mounted in a quasi free–free configuration (without modifying accelerometers configuration) and then its basis is excited instead of the workpiece, thus enabling the measurement of

$$\mathbf{H}(j\omega) = \frac{\mathbf{S}_{dyn}(j\omega)}{\mathbf{A}_{base}(j\omega)} \tag{14}$$

   because in this case $\mathbf{R}_{inp}(j\omega) = 0$ and the quasi free–free conditions imply quasi-impulsive accelerations, which assure a good signal to noise ratio for the identification of $\mathbf{H}(j\omega)$ in a wide frequency range. It is worth noting that this second identification phase – which can be called exogenous training – could be

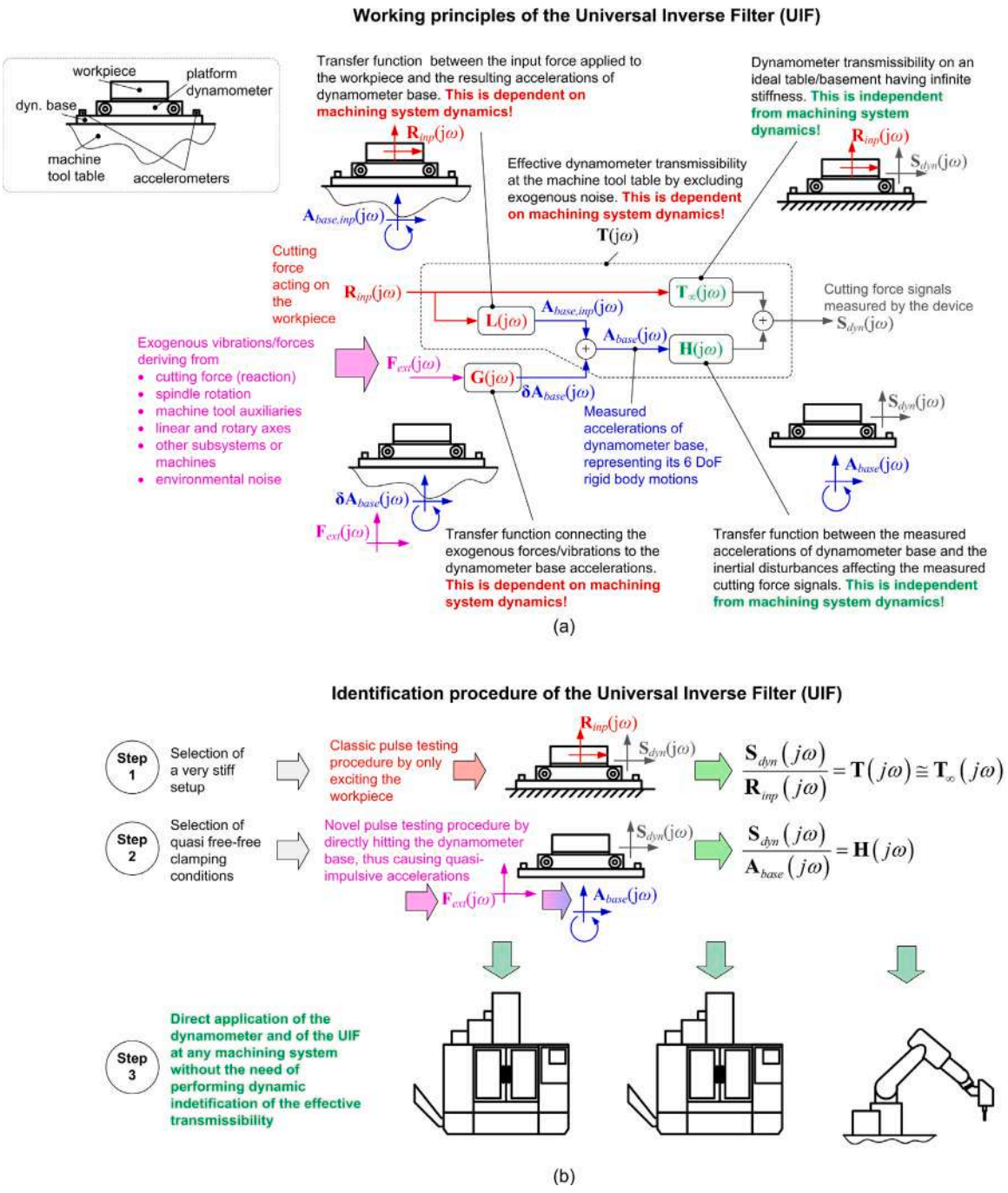

Fig. 2. Scheme representing the effects of input forces applied to the workpiece and exogenous disturbances on the signals measured by the platform dynamometer (a). Modal analysis procedure for the construction of the Universal Inverse Filter (b). The role of dynamometer base accelerations is crucial to understand the principle of the universal dynamometer and how it can compensate for both endogenous and exogenous inertial disturbances.

simply carried out at the same machine tool table of the first phase, by using wax instead of bolts for a soft connection to it. When dynamometer base is excited during the exogenous training, the input forces applied to the workpiece should be set to zero along all directions.

At the end, we are interested in the identification of the following system

$$\begin{aligned}\mathbf{R}_{inp}(j\omega) &= \mathbf{T}_{\infty}(j\omega)^{-1}\left[\mathbf{S}_{dyn}(j\omega) - \mathbf{H}(j\omega)\,\mathbf{A}_{base}(j\omega)\right] \\ &= \mathbf{B}(j\omega)\,\mathbf{S}_{dyn}(j\omega) + \mathbf{C}(j\omega)\,\mathbf{A}_{base}(j\omega)\end{aligned} \tag{15}$$

which expresses the linear relationship in the frequency domain between the target input $\mathbf{R}_{inp}$ and the measured signals $\mathbf{S}_{dyn}$, $\mathbf{A}_{base}$. The coefficients of $\mathbf{B}(j\omega)$ and $\mathbf{C}(j\omega)$ can be derived from a regression procedure carried out in the frequency domain, by exploiting all the experimental data obtained from the modal analysis phases described above, in one single shot. It is worth noting that $\mathbf{B}(j\omega)$ and $\mathbf{C}(j\omega)$ only depend on the transmissibilities $\mathbf{T}_{\infty}(j\omega)$ and $\mathbf{H}(j\omega)$, which are independent from the chosen experimental setup. The two identification phases described above were executed at two radically different configurations, thus forcing the recognition of such configuration-independent transmissibilities, while concurrently canceling the terms which are configuration-dependent, such as $\mathbf{L}(j\omega)$.

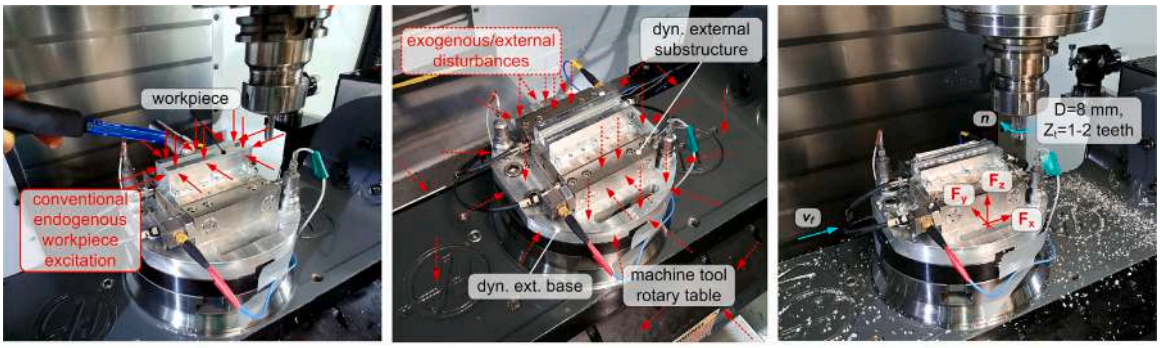

Fig. 3. First phase of modal analysis carried out at a stiff experimental setup, which is an industrial milling machine in the actual case. Internal/endogenous dynamometer excitation by hitting the workpiece (a); external/exogenous excitation by hitting dynamometer base (b); reference scheme for cutting tests (c).

The implementation details of this relatively simple algorithm are explained in the next section.

4. Construction of the universal dynamometer and of the universal inverse filter

4.1. Experimental setup and the new modal analysis procedure

The self-made dynamometer used in [12,14,21] was also adopted here. It has to be recalled that the device is composed of four triaxial piezoelectric force cells Kistler 9016B4, similarly to Kistler Minidyn 9256C2. The measuring chain was also composed of Kistler 5073 charge amplifiers and of an electrical interface supplied by a +24 V generator, thus finally providing ±10 V differential outputs that were sent through coaxial cables to a National Instruments Data Acquisition device (cDAQ-9178 with NI9215 modules).

Contrary to the previous configurations, in the actual case also some piezoelectric accelerometers were attached very close to the dynamometer base, in the perspective of developing an effective accelerometric compensation of the force signals. Specifically, 2 triaxial accelerometers were applied at two opposite corners of dynamometer base (both type PCB 356A25 with sensitivity 25 mV/g), while 2 monoaxial accelerometers (both Kistler 8704B50 with sensitivity 100 mV/g) were attached at the other 2 corners and oriented along the vertical direction.

Thanks to this choice, it was possible to estimate all the 6 rigid body motions $\mathbf{A}_{base}$ of dynamometer base (3 translations and 3 rotations), with some redundancy that helped for increasing the estimate robustness. It is worth noting that the precise accelerometers' locations in the surroundings of dynamometer base are not important, provided that their configuration is sufficient to characterize the rigid body motions of the dynamometer — workpiece subsystem. For any generic accelerometers' positioning, the precise relations between accelerometers signals (representing $\mathbf{A}_{base}$) and the unwanted inertial disturbances affecting the cutting force signals $\mathbf{S}_{dyn}$ will be identified during the novel, generalized modal analysis procedure explained below.

In other words, for a given accelerometers configuration, the precise location and orientation of each sensor is not important, assuming that it is kept constant after the identification phase. In case there are some initial orientation and collocation errors of the accelerometers with respect to their desired nominal positioning, their effects on the final filter will vanish because the proposed method automatically takes into account such errors. No complex calculations are requested to the user (e.g. for estimating workpiece translations and rotations). Of course, accelerometers' configuration should not be modified when the dynamometer is mounted on its final application, otherwise the identification procedure has to be repeated.

An instrumented hammer type Dytran 5800B4 (sensitivity 2.41 mV/N) was used to apply the input forces to the mechanical structure. Input force and acceleration signals were conditioned by Kistler 5134B amplifiers. Sampling frequency was 51.2 kHz for all the signals. The discretized signals were eventually sent and stored on a PC, while the calculations were executed off-line in the MathWorks MATLAB environment.

The workpiece clamped on the central platform of the dynamometer was made of Al7075 aluminum alloy (ERGAL). Its mass was about 130 g and its hardness was about 145 HB. Workpiece geometry was specifically designed to facilitate system excitation at the 16 selected positions as well as to simplify the subsequent cutting tests phase.

In general, important variations of workpiece mass and geometry before and after the material removal process may alter system transmissibilities in a way that cannot be automatically compensated by the developed Universal Inverse Filter. In the following, we will implicitly assume that such variations are sufficiently small to be negligible for our purposes. In another situation, this hypothesis should be carefully verified.

In order to identify and validate the proposed Universal Inverse Filter, modal analysis was executed according to the following procedure.

1. Internal/endogenous training emulating real cutting forces applied to the workpiece was done on a stiff industrial milling machine (HAAS VF-2TR), see Fig. 3, according to the procedure outlined in [12,14], i.e.
   - workpiece excited along X direction by local force $F_1, \dots, F_3$ or F_4;
   - workpiece excited along Y direction by local force $F_5, \dots, F_9$ or F_{10};
   - workpiece excited along Z direction by local force $F_{11}, \dots, F_{15}$ or F_{16};

   This step was crucial to estimate $\mathbf{T}_{\infty}(j\omega)$.
2. Then, exogenous training was executed by hitting dynamometer base at different points and along different directions, under quasi free–free conditions, by attaching the device to an industrial table by means of wax, see Fig. 4. This was essential for a reliable estimation of $\mathbf{H}(j\omega)$.
3. Eventually, the obtained filter was validated on a radically different setup, i.e. on a small and more flexible milling machine which was fully revamped in collaboration with Beckhoff Automation, see Fig. 5.

It is worth noting that both endogenous and exogenous training was repeated on all the three setups, for proving the effectiveness of the filter. However, for the sake of application, only the first two steps described above are really necessary. In Fig. 6 the direct transmissibilities obtained from classic modal analysis (forces applied to the workpiece) are compared. The transmissibilities of the "flexible" milling machine are considerably different from those characterizing the stiff and the

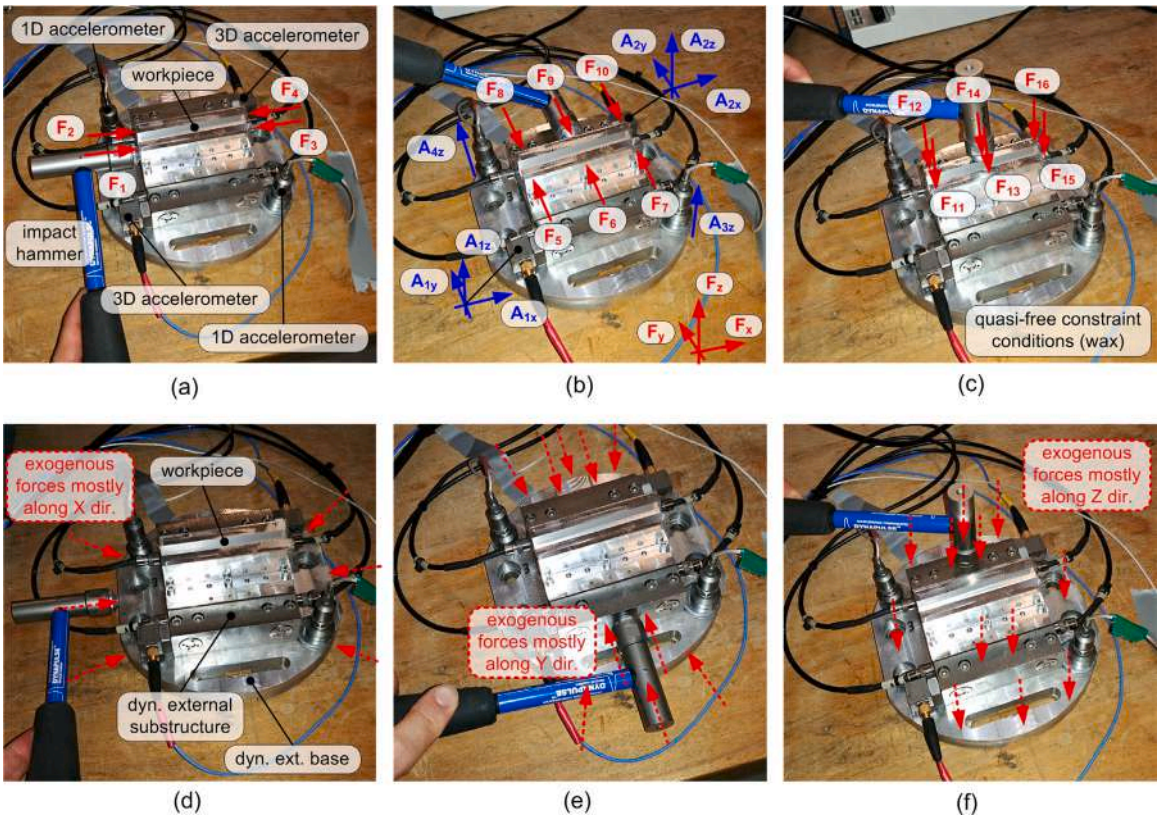

Fig. 4. Second phase of modal analysis carried out under almost free–free constraints, which is an industrial table in the actual case. Internal/endogenous dynamometer excitation by hitting the workpiece in (a), (b) and (c); external/exogenous excitation by hitting dynamometer base in (d), (e) and (f).

quasi free–free clamping conditions. The universal filter developed here will be capable of compensating for the (supposedly unknown) transmissibilities of the flexible machine tool, without the need of measuring them.

The algorithm for filter calculation are described in the next subsection.

4.2. Universal inverse filter calculation

In the light of the theoretical principles introduced in Section 3, and by considering all the data obtained from the first and second pulse testing phases (at the stiff and quasi free–free setups), the new filter was determined according to the following algorithm.

1. All the transients of all the available signals are collected; each transient has the same duration of N samples (here $N \approx 5000$ because the maximum transient lasted ≈ 0.1 s, and the sampling frequency was $f_s \approx 50$ kHz); a total of M transients is collected (here $M \approx 200$), including all the possible excitation conditions illustrated in the previous subsection. This is essential to achieve the final result. Some preliminary basic pre-processing is also recommended here. In the current case, less than 5 min were required for this step (on a conventional workstation).
2. The Discrete Fourier Transform of each transient of each signal is computed, without truncation or zero padding. In the current case, less than 10 s were required for this step.
3. For each discrete pulsation ω_k, the following algebraic system of complex entries is assembled

$$\begin{bmatrix} \widetilde{R}^{(1)}_{x,k} & \widetilde{R}^{(1)}_{y,k} & \widetilde{R}^{(1)}_{z,k} \\ \widetilde{R}^{(2)}_{x,k} & \widetilde{R}^{(2)}_{y,k} & \widetilde{R}^{(2)}_{z,k} \\ \vdots & \vdots & \vdots \\ \widetilde{R}^{(M)}_{x,k} & \widetilde{R}^{(M)}_{y,k} & \widetilde{R}^{(M)}_{z,k} \end{bmatrix} = \begin{bmatrix} \widetilde{S}^{(1)}_{1,k} & \cdots & \widetilde{S}^{(1)}_{Q,k} & \widetilde{A}^{(1)}_{1,k} & \cdots & \widetilde{A}^{(1)}_{Q',k} \\ \widetilde{S}^{(2)}_{1,k} & \cdots & \widetilde{S}^{(2)}_{Q,k} & \widetilde{A}^{(2)}_{1,k} & \cdots & \widetilde{A}^{(2)}_{Q',k} \\ \vdots & & \vdots & \vdots & & \vdots \\ \widetilde{S}^{(M)}_{1,k} & \cdots & \widetilde{S}^{(M)}_{Q,k} & \widetilde{A}^{(M)}_{1,k} & \cdots & \widetilde{A}^{(M)}_{Q',k} \end{bmatrix} \times \begin{bmatrix} \widetilde{B}_{x,1,k} & \widetilde{B}_{y,1,k} & \widetilde{B}_{z,1,k} \\ \vdots & \vdots & \vdots \\ \widetilde{B}_{x,Q,k} & \widetilde{B}_{y,Q,k} & \widetilde{B}_{z,Q,k} \\ \widetilde{C}_{x,1,k} & \widetilde{C}_{y,1,k} & \widetilde{C}_{z,1,k} \\ \vdots & \vdots & \vdots \\ \widetilde{C}_{x,Q',k} & \widetilde{C}_{y,Q',k} & \widetilde{C}_{z,Q',k} \end{bmatrix} \tag{16}$$

where $\widetilde{R}^{(m)}_{x,k} \in \mathbb{C}$ is the Discrete Fourier Transform (DFT) of $R_x \in \mathbb{R}$ corresponding to the mth transient ($m = 1, 2, \ldots, M$), evaluated at the discrete pulsation ω_k, $\widetilde{S}^{(m)}_{q,k}$ is the DFT of dynamometer signal S_q corresponding to the mth transient, evaluated at ω_k and similarly for $\widetilde{A}^{(m)}_{q,k}$. Eventually, $\widetilde{B}_{w,q,k}$ and $\widetilde{C}_{w,q',k}$ ($w = x, y, z$) are the filter responses in the frequency domain, evaluated at pulsation ω_k, which are associated to dynamometer signals S_q and to acceleration signals $A_{q'}$ respectively, for the reconstruction of the resultant force component R_w. In other words, Eq. (16) is the algebraic representation of Eq. (15) for a given discrete pulsation ω_k. The typical size of the coefficient matrix used for computing the pseudoinverse is small ($M \times (Q + Q')$), i.e. proportional to the number of transients, which is about $M \approx 200$. This poses no numerical problems when computing the pseudoinverse. This is one great advantage of working in the frequency domain (contrary to the URDF approach), because frequency domain allows the best, optimal diagonalization of the original problem, as explained in [14].

The Truncated Singular Value Decomposition (TSVD) is applied to regularize this system, and then the pseudoinverse is computed. The pseudoinverse is used to determine the unknowns $\widetilde{B}_{w,q,k}$ and $\widetilde{C}_{w,q',k}$. The same procedure is iterated for all the other pulsations ω_k, with $k = 1, \ldots, N$. In the current case, less than 15 s were required for this step (whereas URDF may require 30 min or much more, when it is possible to apply it).

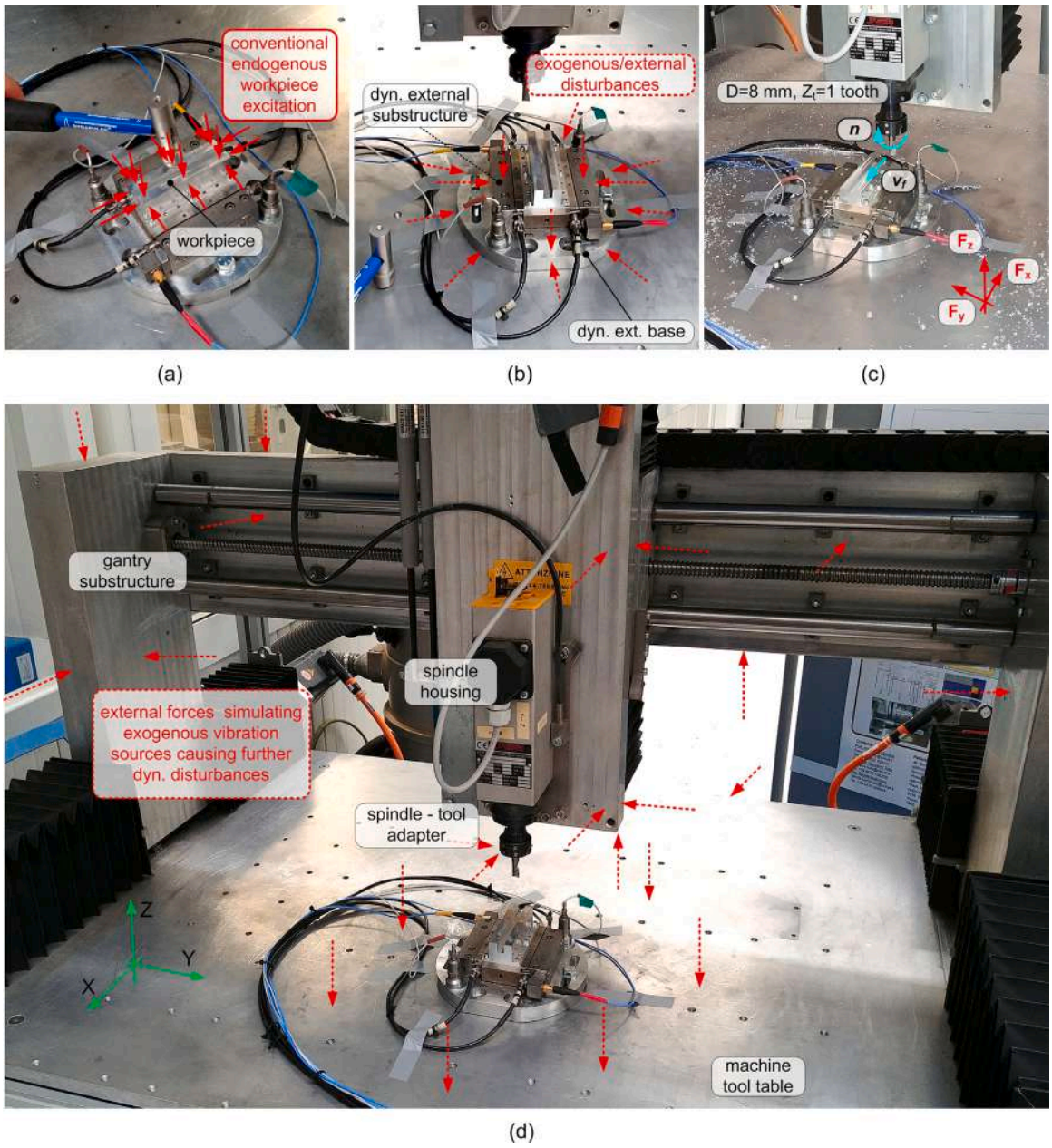

Fig. 5. Validation of the Universal Inverse Filter at a generic milling machine, which is the "flexible" milling machine endowed with Beckhoff automation in the actual case. Internal/endogenous dynamometer excitation by hitting the workpiece (a); external/exogenous excitation by hitting dynamometer base (b); further tests by applying impulsive disturbances to the machine tool structure (d); reference scheme for the final cutting tests (c).

4. Afterwards, each Finite Impulse Response composing the filter is reconstructed through the Inverse Discrete Fourier Transform of the sequence

$$B_{w,q,n} = \frac{1}{N}\sum_{k=1}^{N} \widetilde{B}_{w,q,k} e^{j\frac{2\pi}{N}(m-1)(k-r)}, \quad r \cong \frac{N}{2} \tag{17}$$

where $w = x, y, z$, $q = 1, \dots, Q$ and $n = 1, \dots, N$. Similarly, $C_{w,q',n}$ is obtained from the sequence $\widetilde{C}_{w,q',k}$, for $w = x, y, z$ and for any $q' = 1, \dots, Q'$. To smooth undesired noise affecting the initial and final tails of the impulse responses, the Hanning window is also applied to each of them. For the sake of clarity, the size of the matrix representing the filter for a given pulsation ω_k is $3 \times (Q + Q')$, because the 3 filtered global force components are derived from $Q + Q'$ signals. In detail, the matrix size will be

- 3×3 when constructing the classic OIF for a commercial dynamometer, where only 3 unfiltered global force components are available;
- 3×12 when constructing the more advanced SOIF based on $Q = 12$ signals derived from 4 triaxial load cells;
- $3 \times (3 + 8)$ when generating the novel UIF for a commercial dynamometer providing $Q = 3$ raw, global force components considered together with $Q' = 8$ acceleration signals;

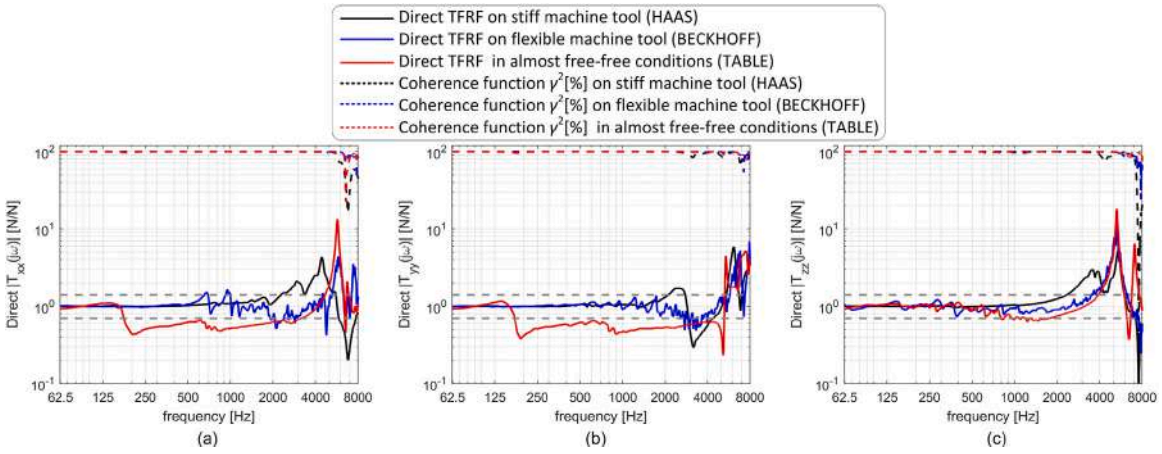

Fig. 6. Experimental direct transmissibilities corresponding to the three experimental configurations that were investigated in this work: stiff machine tool (Haas), flexible machine tool (Beckhoff) and free–free conditions (table). It is worth noting that the results are quite different, thus proving the universality of the proposed filter.

- $3 \times (12 + 8)$ when computing the novel UIF for a special dynamometer providing all the $Q = 12$ load cells' signals considered together with $Q' = 8$ acceleration signals.

In the current case less than 0.1 s were required for this step.

5. Eventually, the filter can be applied the measured signals through a linear convolution in the time domain, as follows

$$R_w(\cdot) = \sum_{q=1}^{Q} B_{w,q}(\cdot) * S_q(\cdot) + \sum_{q'=1}^{Q'} C_{w,q'}(\cdot) * A_{q'}(\cdot) \tag{18}$$

It is worth noting that the above procedure is much simpler and more straightforward than that proposed for SOIF in [14] and that proposed for URDF in [12]. SOIF and URDF were based on a preliminary determination of all the transfer functions of the global $Q \times P$ transmissibility matrix representing dynamometer dynamics (without accelerometers). In the former research works the importance of exciting $P = 16$ distinct points on the workpiece was highlighted, with the aim of a correct filter construction. Also in the current case it is important to excite the workpiece at different locations – for a given force direction – in order to train the system to recognize a given force component independently from its location on the workpiece. Nevertheless, here the final regression algorithm used for filter construction practically eliminates the formal distinction among the P points. Only the 3 different directions of the input force remain formally independent and distinct in Eq. (16). Thus, for the sake of simplicity the parameter P will be suppressed in the following, whereas the type and number of measured signals $Q + Q'$ will be emphasized to distinguish the different filtering approaches.

It has to be also recalled that the repeated application of the Singular Value Decomposition was used to compress the $Q \times P$ transmissibility matrix before filter construction in the former works. Such compression was not only a more compact re-formulation of the problem, but it was necessary to reduce the computational burden required by URDF. In contrast, a posteriori it can be noticed that it was not strictly necessary for SOIF, because its frequency domain representation was already sufficient to achieve the desired problem compression.

According to Eq. (11), dynamometer signals S_q are the consequence of both the effective input forces $R_{inp,w}$ applied to the workpiece and the measured accelerations $A_{q'}$ of dynamometer base. Ideally, to estimate all the transmissibilities between each input and each output, the system should be stimulated by one input at a time, setting all the others to zero. However, this was not feasible because the accelerations of the dynamometer base are excited by the forces acting on the workpiece as well, preventing them from being simultaneously set to zero. In other words, some input types are strongly correlated among each other and cannot be physically decoupled.

To address this issue, the system was reformulated in the inverse form (15), which expresses the mathematical relationship between the effective input forces acting on the workpiece and the available force and acceleration signals. This is a simple linear combination in the frequency domain. For any frequency, the final regression system (16) is ill-conditioned because of the correlations among dynamometer and accelerometers' signals. Thus, regularization through Singular Value Decomposition (SVD) is necessary before computing the pseudo-inverse to obtain reliable filter coefficients. However, in general it is important to provide a comprehensive dataset to (16), which should be representative of all possible endogenous and exogenous system excitations, to obtain an effective linear map for cutting force reconstruction.

5. Validation through modal analysis

The Universal Inverse Filter (UIF) was computed and cross-validated on the flexible milling machine by applying

- endogenous forces to the workpiece;
- exogenous forces to the dynamometer base;
- further undesired inertial disturbances triggered by generic impulsive forces at
  - the cutting tool/spindle/spindle housing;
  - the gantry substructure;
  - the machine tool table;
  - the same as in the previous point, during simultaneous linear axes rapid movements and spindle rotation.

In order to demonstrate the effectiveness of the new UIF, its results were compared to the signals derived from other filtering techniques, as follows.

1. **HAMMER**: effective input forces estimated by the instrumented hammer (available only during modal analysis).
2. **RAW**: global force components obtained from static calibration without filtering.
3. **OIF** ($Q = 3, Q' = 0$): only the 3 global force components are derived from the sensing device, which are given as inputs to the filter for force reconstruction; only endogenous training is carried out (forces applied to the workpiece); identification and validation are directly executed on the target milling machine (i.e. the small and relatively flexible milling machine).
4. **SOIF** ($Q = 12, Q' = 0$): all the 12 load cells' signals are available for force reconstruction, but no accelerometers are present; only classic endogenous training is carried out; identification and validation are directly executed on the target milling machine.

5. **Basic, reference UIF** ($Q = 3, Q' = 8$): 3 global force components are available for force reconstruction together with 8 acceleration signals; both endogenous and exogenous training are carried out; identification and validation are executed on the target milling machine.
6. **Advanced, reference UIF** ($Q = 12, Q' = 8$): all the 12 load cells' signals are available plus the 8 acceleration signals; both endogenous and exogenous training are carried out; identification and validation are executed on the target milling machine.
7. **Basic, cross-validated UIF** ($Q = 3, Q' = 8$): 3 global force components are available for force reconstruction together with 8 acceleration signals; both endogenous and exogenous training are carried out; identification is executed at the stiff and quasi free–free conditions, while validation is performed at the target milling machine.
8. **Advanced, cross-validated UIF** ($Q = 12, Q' = 8$): all the 12 load cells' signals are available plus the 8 acceleration signals; both endogenous and exogenous training are carried out; identification is executed at the stiff and quasi free–free conditions, while validation is performed at the target milling machine.

OIF and SOIF represent state of the art approaches which do not take into account accelerometers' signals and are only based on classic endogenous training (cutting forces applied to the workpiece). It has to be recalled that the effective, non-parametric Upgraded Regularized Deconvolution Filter (URDF) could not be applied because it required an excessive memory consumption, far beyond the possibilities of a conventional workstation.

On the other side, UIF filters are based on accelerometers' signals as well as on both endogenous and exogenous training. The best performance is expected from the basic and advanced UIFs which have been identified and validated on the same target machine. However, the cross-validated UIFs are the most important versions because they emulate the real use of the UIF, which should be calibrated by the manufacturer and then applied by a possibly non-expert user to any machine tool without repeating the identification phase.

It is worth recalling that both commercial dynamometers based on 3×3 transmissibility models as well as special, taylor-made dynamometers derived from linear combinations of Q force signals (in the current case $Q = 12$) may benefit from this algorithm. UIF can even be implemented a posteriori by the final user on any type of dynamometers, by simply attaching a sufficient number of accelerometers to the dynamometer base.

In general, all the filters were expressed in the frequency domain as a sequence of about $N = 5000$ matrices of appropriate size, depending on the considered approach.

No preliminary compression steps through the SVD technique were applied in the time domain, as done in the former work [14]. Such compression was not even feasible because force and acceleration signals were dynamically coupled during the pulse tests. Thus, SVD was directly applied in the frequency domain, just once for each pulsation, before the pseudoinverse calculation.

In Fig. 7 some impulse responses are shown, where the input force is applied along different directions, in the presence of exogenous disturbances.

As expected, state of the art filters (OIF/SOIF) are capable of suppressing the inertial disturbances owing to the input forces applied to the workpiece, when no other inputs are applied. However, they need to perform modal analysis when the device is mounted at the final machine tool. Moreover, they are ineffective in the presence of exogenous disturbances. For overcoming these disadvantages the UIF was developed, which takes into account the acceleration signals and which is based on both endogenous and exogenous training. By so doing, the filtered signals are almost coincident to the true inputs (hammer) along the direct directions, and cross-talk disturbances are effectively minimized. The differences among the reference and cross-validated UIFs are practically negligible.

Similar conclusions can be drawn from the analysis of the compensated transmissibilities, which are shown in Fig. 8. Direct TFRFs are well compensated while cross TFRFs are well attenuated up to about 4–5 kHz.

For the sake of quantifying the performance of the different methods in the frequency domain, the following criteria were adopted:

- the usable frequency bandwidth of the direct TFRFs were determined from the classic ±3 dB thresholds with respect to the ideal unitary gain;
- the usable frequency bandwidth of the cross TFRFs were determined by considering a threshold equal to 0.25, by recalling that the cross TFRF should be ideally zero.

The achieved frequency bandwidths along direct and cross directions are illustrated in Fig. 9(a). The novel, reference UIF reaches on average 6.5 kHz along direct directions (similarly to OIF/SOIF) and 4.5 kHz along cross directions (more than 4 times better than OIF/SOIF). Satisfactory results are finally confirmed by the cross-validated UIFs, on average 5 kHz along direct directions and 4 kHz along cross directions, thus proving the effectiveness of the proposed universal filter. The same conclusion can be drawn from Fig. 9(c), where the minimum cross disturbances were obtained by the UIF. The better behavior of the novel method is also proved by the higher squared linear correlation coefficients of Fig. 9(b).

Eventually, different kinds of cross-talk errors before and after UIF compensation are illustrated in Fig. 10. When they derive from exogenous disturbances, application of UIF is crucial for their correction.

6. Validation through cutting tests

6.1. Experimental design and identification of a reference cutting force model

Several cutting tests were carried out to assess the capabilities of cutting force reconstruction by the Universal Inverse Filter during an actual cutting process.

All cutting tests were replicated on the two milling machines investigated in the previous phase, i.e.

- the stiff milling configuration (HAAS VF-2TR, Fig. 3(c)) and
- the relatively flexible, small milling machine equipped with Beckhoff automation (Fig. 5(c)).

It is worth recalling that the preliminary UIF calibration was derived from the first configuration and from the table configuration illustrated in Fig. 4, while the flexible milling machine was adopted for the final validation, as done here through the cutting tests. No significant exogenous disturbances affected the milling operations executed at the stiff milling machine. For all these reasons, the results obtained from the stiff milling machine were taken as a reference for assessing filter performances in the final configuration.

On each machine, two different cutting tool geometries were tested, i.e.

1. Sandvik Coromant cylindrical endmill 2P230-0800-NA H10F having $D = 8$ mm of external diameter, $Z_t = 1$ active tooth, a negligible nose radius $r_\varepsilon \leq 0.1$ mm, normal rake angle $\gamma_n = 13.5°$ and an axial rake angle $\gamma_a = 30°$.
2. Sandvik Coromant bull-nose cutter 2S220-0800-100-NC H10 having $D = 8$ mm of external diameter, $Z_t = 2$ active teeth (which were reduced to 1 in some cases, as explained below), nose radius $r_\varepsilon = 1$ mm, normal rake angle $\gamma_n = 17°$ and an axial rake angle $\gamma_a = 30°$.

For each machine tool and cutting tool type, different cutting conditions were investigated, according to the Design of Experiments reported in Table 1, including quasi-slotting conditions, central milling

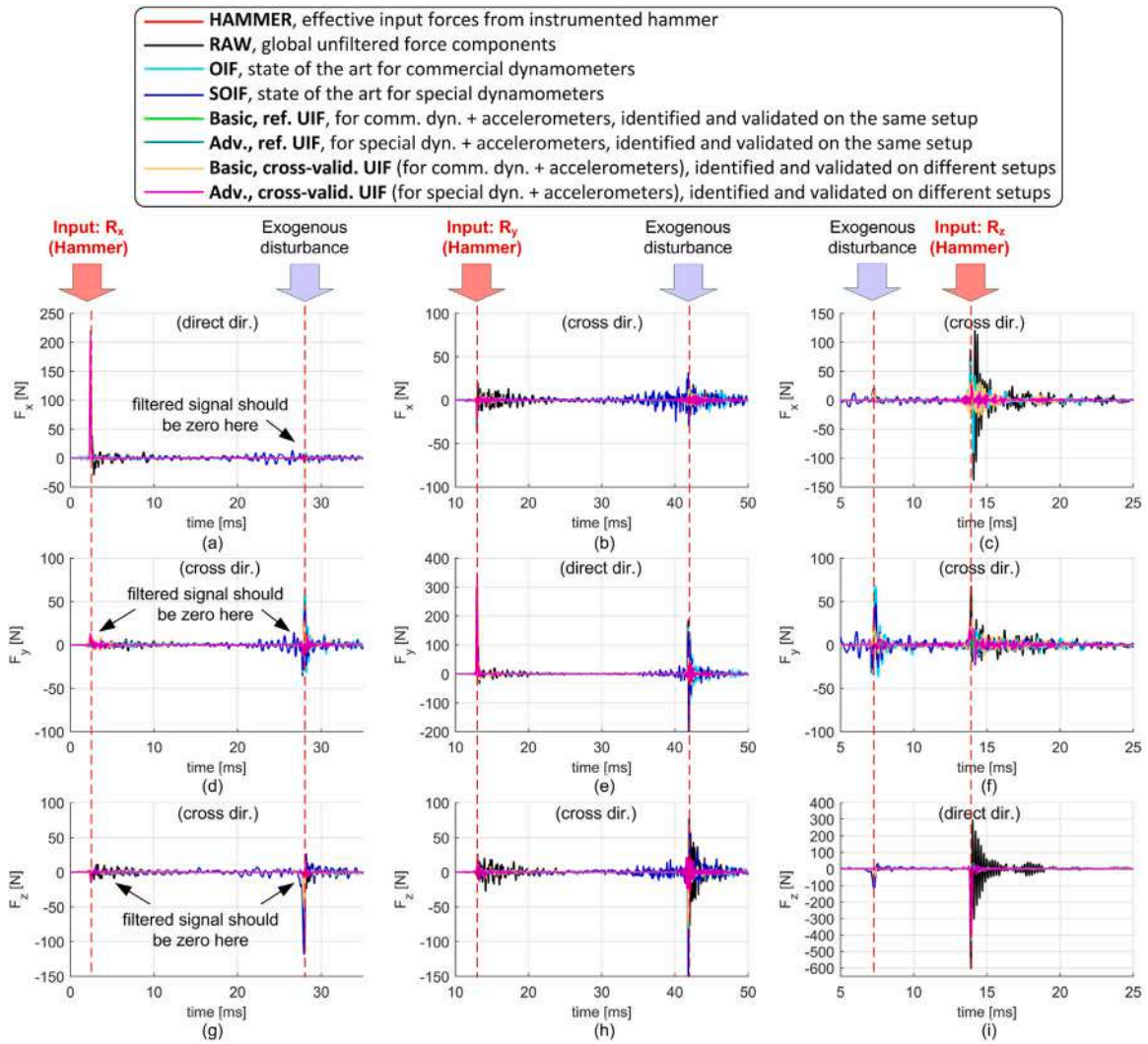

Fig. 7. Examples of filtered impulse responses along the three main directions, when applying different filtering approaches. Please notice that there are 3 distinct conditions, one for each sensing direction. On the left, only one direct input along X direction is applied, plus an exogenous noise ((a), (d), (g)). In the center, only one direct input along Y direction is applied, plus and exogenous disturbance ((b), (e), (h)). Eventually, on the right a direct impulse along Z direction is applied, plus an exogenous disturbance (this time, before the direct input) ((c), (f), (i)). The cross-validated Universal Inverse Filter is capable of reconstructing the effective input by concurrently canceling undesired exogenous noise.

of a thin walled structure, peripheral down and up milling tests described by different combinations of the lateral engagement parameters a_{L1} and a_L. Such different cutting conditions gave rise to different cutting force trends, thus increasing the robustness of the estimated cutting force model coefficients.

For most combinations of cutting parameters listed in Table 1 - corresponding to a fractional, factorial Design of Experiments - a complete milling pass was executed to verify filters' effectiveness at different tool-workpiece contact positions. When replicating the tests at the small, flexible milling machine, the machine tool structure was hit by external forces during the cutting process to simulate the effect of exogenous disturbances. A total of about 80 cutting tests were executed.

For evaluating filters' performances, filtered forces were compared to theoretical cutting force trends simulated by a conventional Shearing & Ploughing cutting force model, as done in [12]. The model was calibrated in the stiffer milling configuration and then used in the final configuration, without repeating the identification phase of the mechanistic model coefficients.

For this purpose, let us first neglect the presence of the nose radius r_ε and let us assume constant pitch, regular helicoidal teeth having a uniform cutting edge angle $\chi = 90°$ and axial rake angle $\gamma_a = 30°$ along the cutting edge. Let us consider the generic cutting edge element of the jth tooth, whose position is given by the feed motion angle φ_j of the flute tip and by the axial coordinate z of the flute element (having axial extension dz). The infinitesimal forces acting on such element can be approximated by the following expression

$$\begin{cases} dF_{cj} \cong g_j \left(k_{cs} dA_j + k_{cp} dz\right) \\ dF_{rj} \cong g_j \left(k_{rs} dA_j + k_{rp} dz\right) \\ dF_{aj} \cong g_j \left(k_{as} dA_j + k_{ap} dz\right) \end{cases} \tag{19}$$

where dF_{cj}, dF_{rj} and dF_{aj} are the infinitesimal forces along the tangential, radial and axial directions, respectively; g_j is the window function representing the engagement between such cutting edge element and the workpiece; dA_j is the infinitesimal uncut chip section area of the considered cutting edge element; k_{cs}, k_{rs} and k_{as} [N/mm^2] are the shearing coefficients in the tangential, radial and axial directions and similarly k_{cp}, k_{rp} and k_{ap} [N/mm] are the ploughing coefficients in the tangential, radial and axial directions, as done in [40].

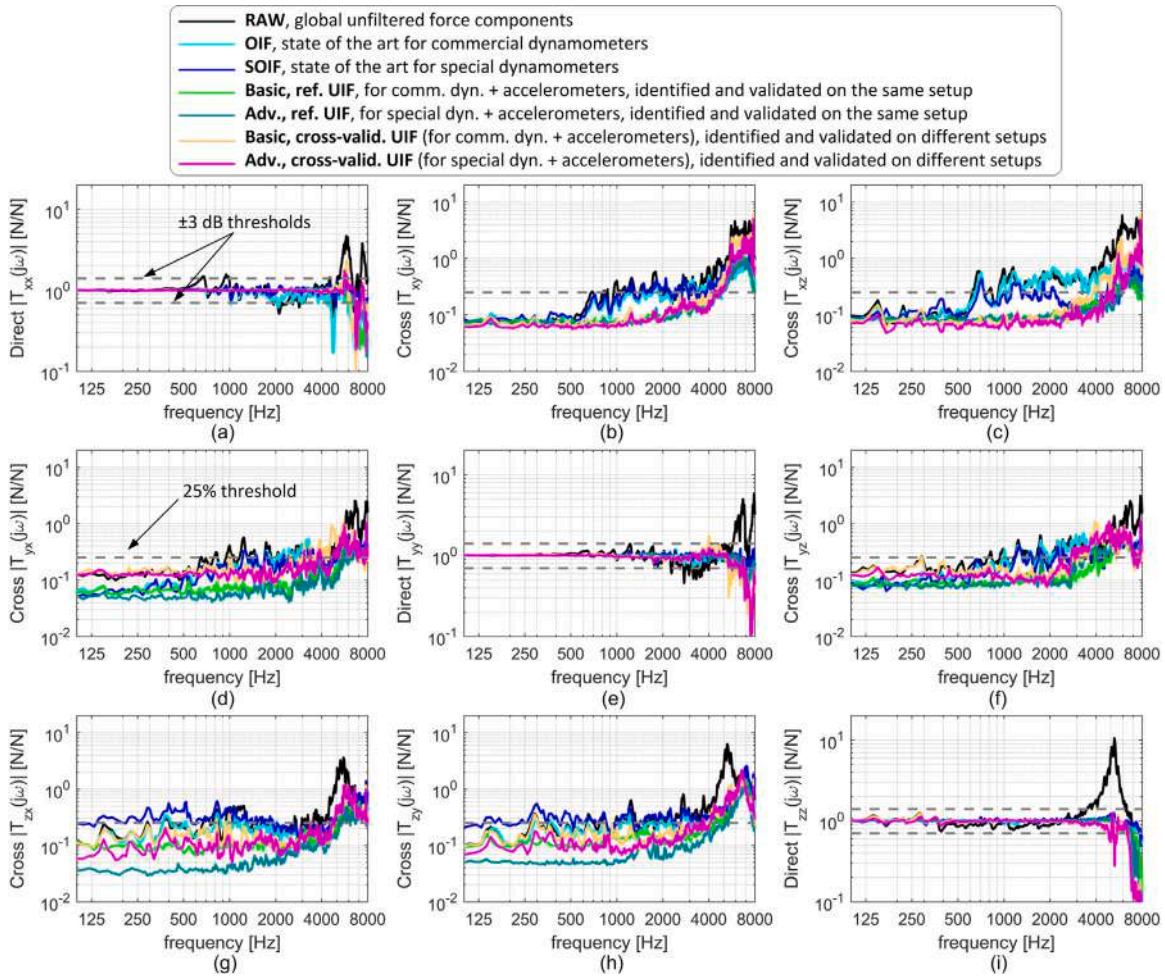

Fig. 8. Transmissibilities Frequency Response Functions (TFRFs) obtained along direct and cross directions from the applications the novel approach versus state of the art approaches. The best performance of the novel approach is overt.

Table 1
Design of Experiments for cutting tests.

Factor	Levels	Values
Milling machine tool type	2	stiff mach.(HAAS VF2TR); flex. mach.(Beckhoff)
Cutting tool type	2	cylindrical endmill; bull-nose cutter
Spindle speed n [rpm] (cutting speed v_c [m/min])	3	10000(251), 15000(377), 24000(603)
Feed per tooth f_z [mm]	2	0.05, 0.1
Depth of cut a_p [mm]	3	0.6, 1.2, 1.8
Lateral tool-workpiece immersion (a_{L1}, a_L) [mm]	4	(2.5,6.5), (−3.5,0.5), (4,0.5), (1,2)

Eventually, the components of the resultant force can be computed by projecting the infinitesimal terms along X, Y and Z and then summing together all the terms along each flute

$$\begin{cases} R_x = \sum_{j=1}^{z_t} \int_{z=0}^{a_p} -dF_{cj}\cos\varphi_j - dF_{rj}\sin\varphi_j \\ R_y = \sum_{j=1}^{z_t} \int_{z=0}^{a_p} dF_{cj}\sin\varphi_j - dF_{rj}\cos\varphi_j \\ R_z = \sum_{j=1}^{z_t} \int_{z=0}^{a_p} dF_{aj} - \sum_{j=1}^{z_t} g_j(\varphi_j)\, k_{ar_\varepsilon} r_\varepsilon \end{cases} \tag{20}$$

where the axial component of the resultant R_z was corrected (for $z > r_\varepsilon$) in order to take into account the presence of the nose radius r_ε by means of an additional, ad hoc coefficient k_{ar_ε} expressed in [N/mm]. This model was inspired by the well established cutting force model developed in [41] in the presence of a significant nose radius. It is worth noting that the sign of all the components was reversed here, thus the forces of the following figures are those acting on the dynamometer, which are the opposite of those acting on the tool.

The mechanistic S&P cutting force model coefficients were firstly estimated from the data measured in the stiff milling configuration (HAAS VF-2TR). The obtained values are reported in Table 2. By comparing the simulated cutting forces with the filtered forces, a satisfactory correlation was found: squared linear correlation coefficients higher than about 0.95 along the most important and energetic directions, i.e. X and Y. The worse performance along the axial direction was caused by the small axial forces. This good agreement is visible in Fig. 11 and in Fig. 12.

A slightly worse agreement was found in the case of the bull nose cutter – see Fig. 13 – because of the unavoidable teeth run-out. For this reason, a bull nose cutter having only one active tooth (the other was ground away) was used in the subsequent cutting tests executed at the smaller milling machine, whose large spindle eccentricity (more than 0.05 mm) would have caused an excessive difference among the teeth.

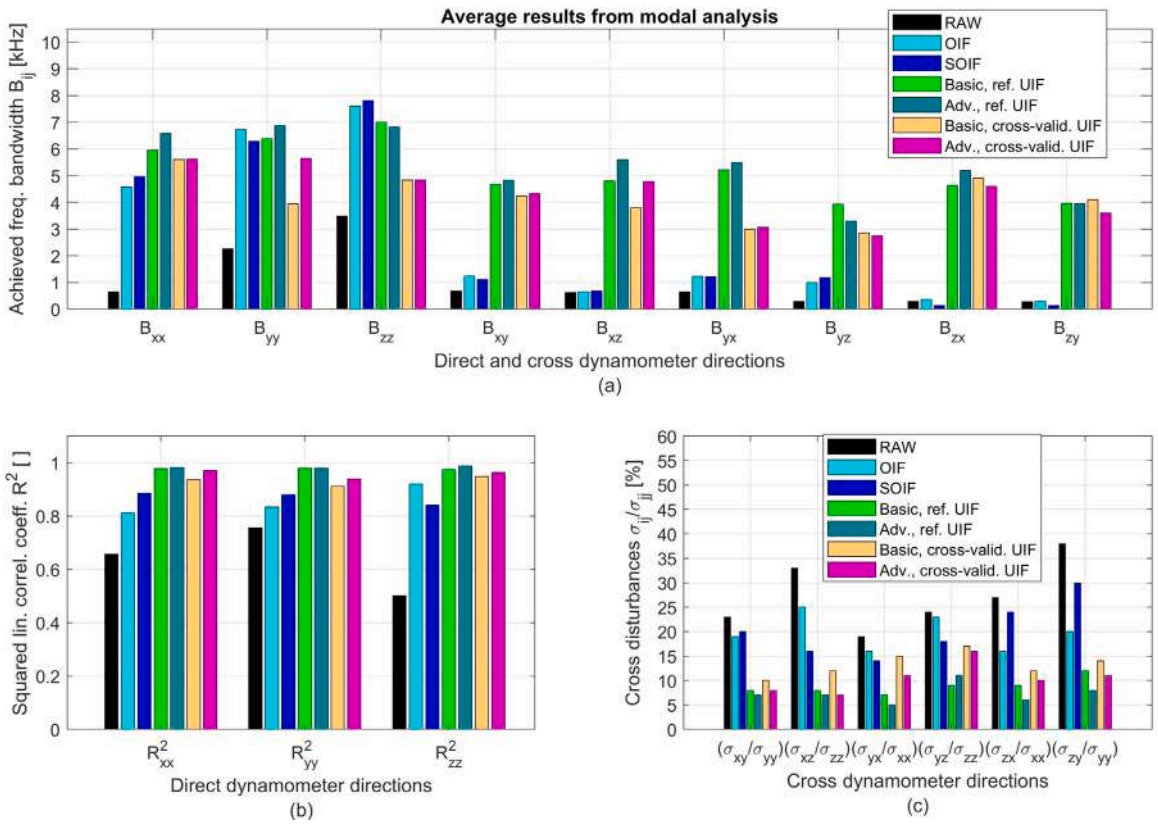

Fig. 9. Performance indicators derived from modal analysis. The Universal inverse Filter exploiting accelerometric compensation trained by means of both internal and external forces outperforms the state of the art approaches, i.e. the Optimal inverse Filter (OIF) and the Superior Optimal inverse Filter (SOIF) in terms of achieved frequency bandwidths (especially along the cross directions, see (a)), squared linear correlation coefficients of the reconstructed forces w.r.t. the effective input force components (b) and cross-talk disturbances (c).

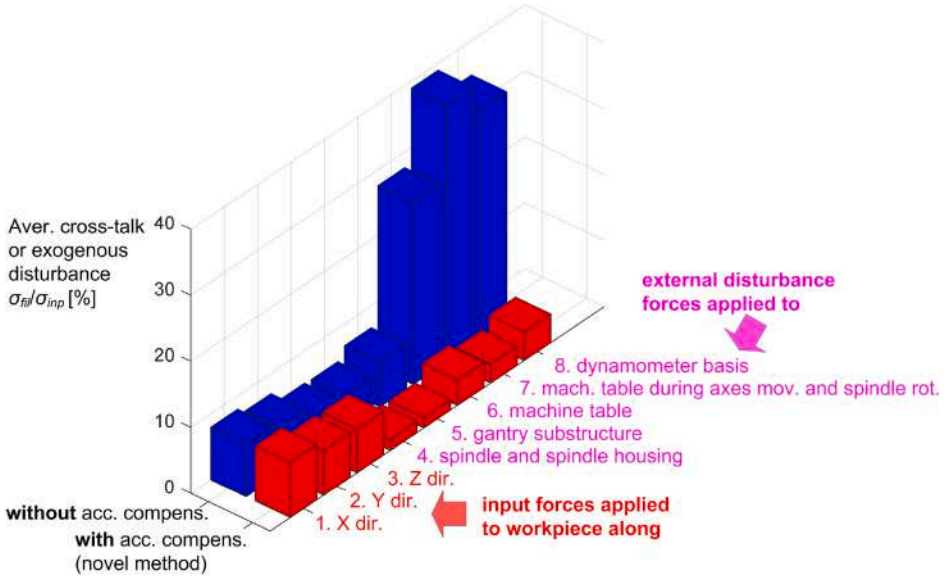

Fig. 10. Qualitative illustration of the main sources of external/exogenous disturbances that may negatively affect dynamometer transmissibilities: cutting forces applied to tooling system, vibrations due to spindle rotations, vibrations due to linear axes movements and vibrations that may possibly derive from other actuators located on machine tool table or close to the dynamometer location.

Table 2
Cutting force model coefficients estimated from the measurements at the stiff milling machine.

Tool type	k_{cs} [MPa]	k_{rs} [MPa]	k_{as} [MPa]	k_{cp} [N/mm]	k_{rp} [N/mm]	k_{ap} [N/mm]	k_{ar_ϵ} [N/mm]
Cylindrical endmill	725.8	290.2	87.1	21.9	19.6	3.8	40.2
Bull-nose cutter	565.2	104.1	52.0	13.2	8.9	7.9	16.0

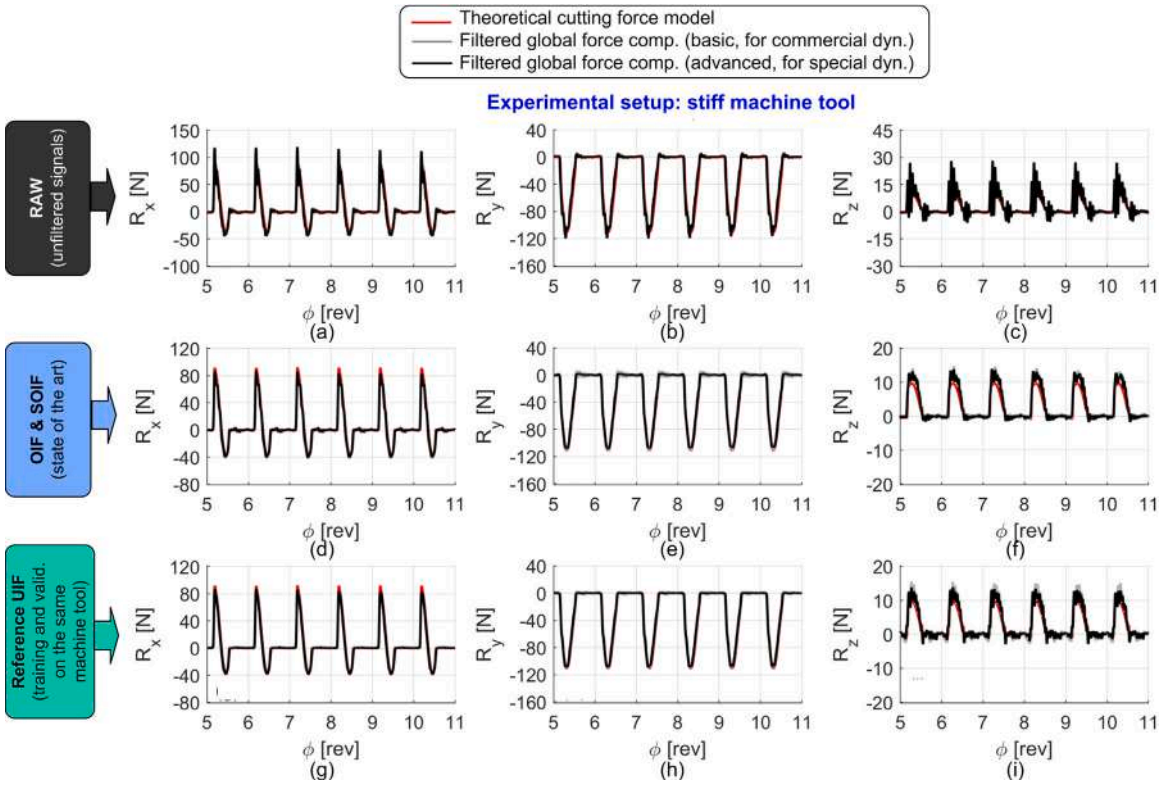

Fig. 11. Comparison between the force components reconstructed from the different filters, under quasi-slotting milling conditions with the cylindrical endmill at the stiff machine tool (HAAS). Nominal cutting parameters: $n = 15\,000$ rpm, $f_z = 0.1$ mm, $a_p = 1.2$ mm, $a_{L1} = 2.5$ mm, $a_L = 6.5$ mm.

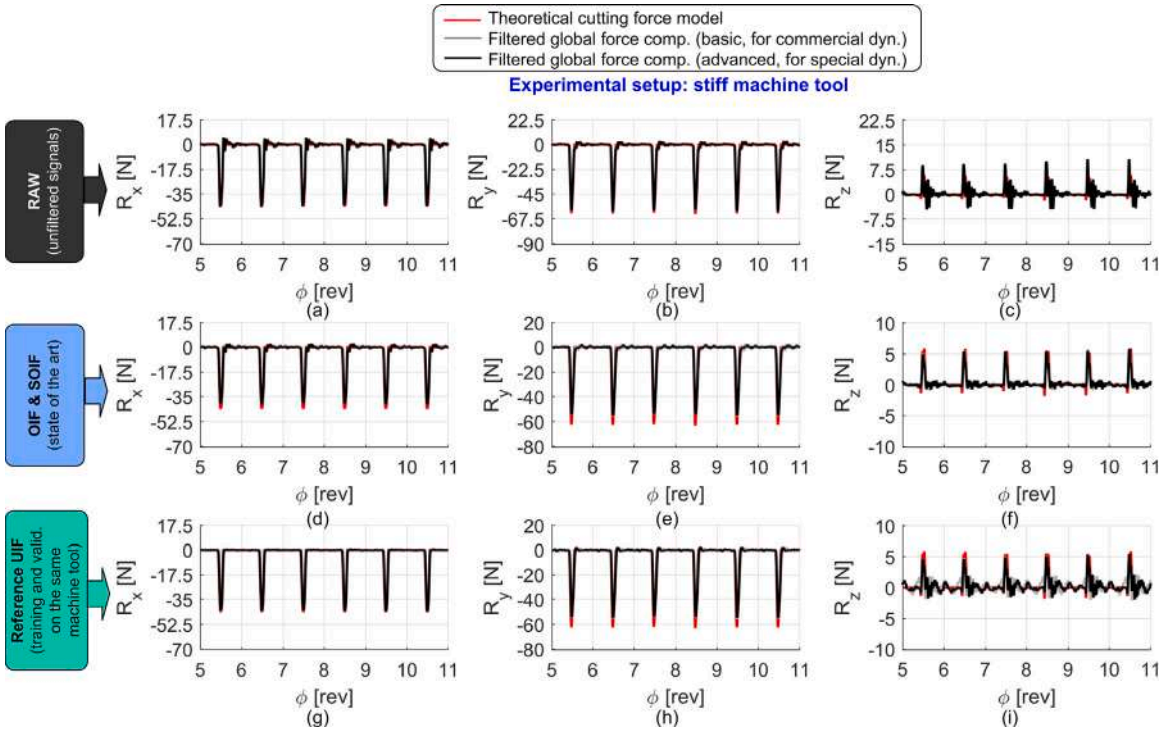

Fig. 12. Comparison between the force components reconstructed from the different filters, under peripheral down milling with the cylindrical endmill at the stiff machine tool (HAAS). Nominal cutting parameters: $n = 15\,000$ rpm, $f_z = 0.05$ mm, $a_p = 1.8$ mm, $a_{L1} = -3.5$ mm, $a_L = 0.5$ mm.

Accordingly, the theoretical S&P force model was adopted as a reference for assessing filters' performances in the final, more flexible and noisy experimental configuration, without repeating the regression procedure on the data obtained from such configuration. In other words,

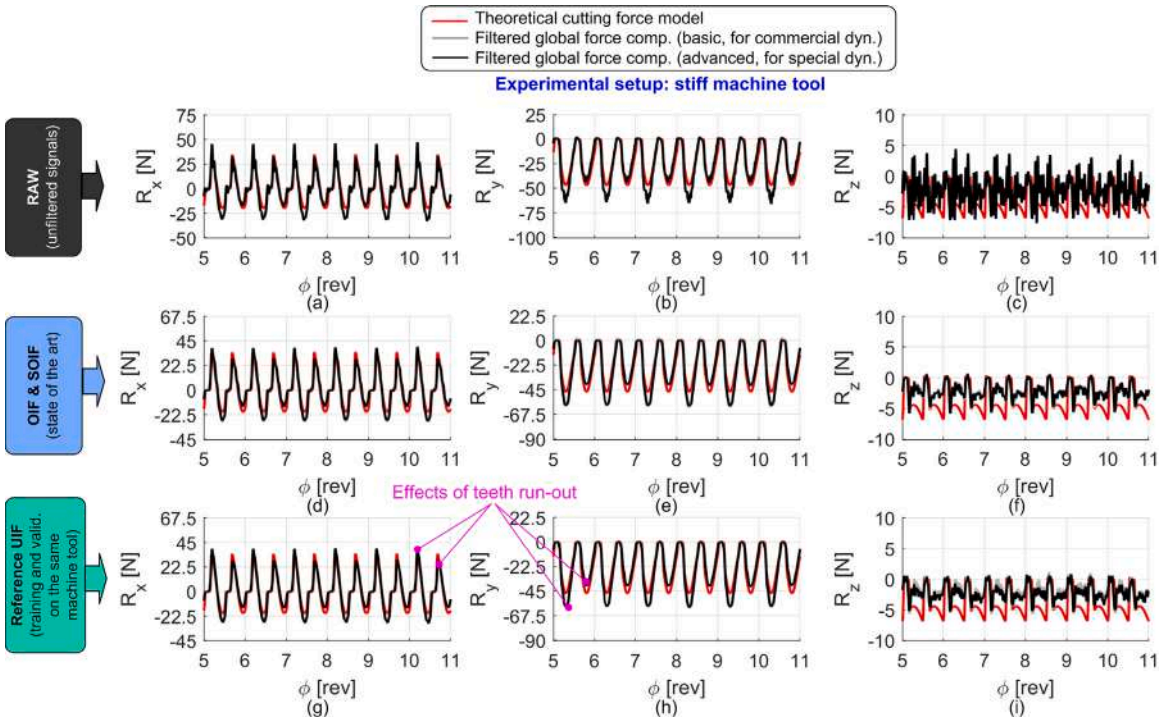

Fig. 13. Comparison between the force components reconstructed from the different filters, under quasi slotting conditions with the bull nose cutter (with 2 active teeth) at the stiff machine tool (HAAS). Nominal cutting parameters: $n = 15\,000$ rpm, $f_z = 0.05$ mm, $a_p = 1.2$ mm, $a_{L1} = 2.5$ mm, $a_L = 6.5$ mm.

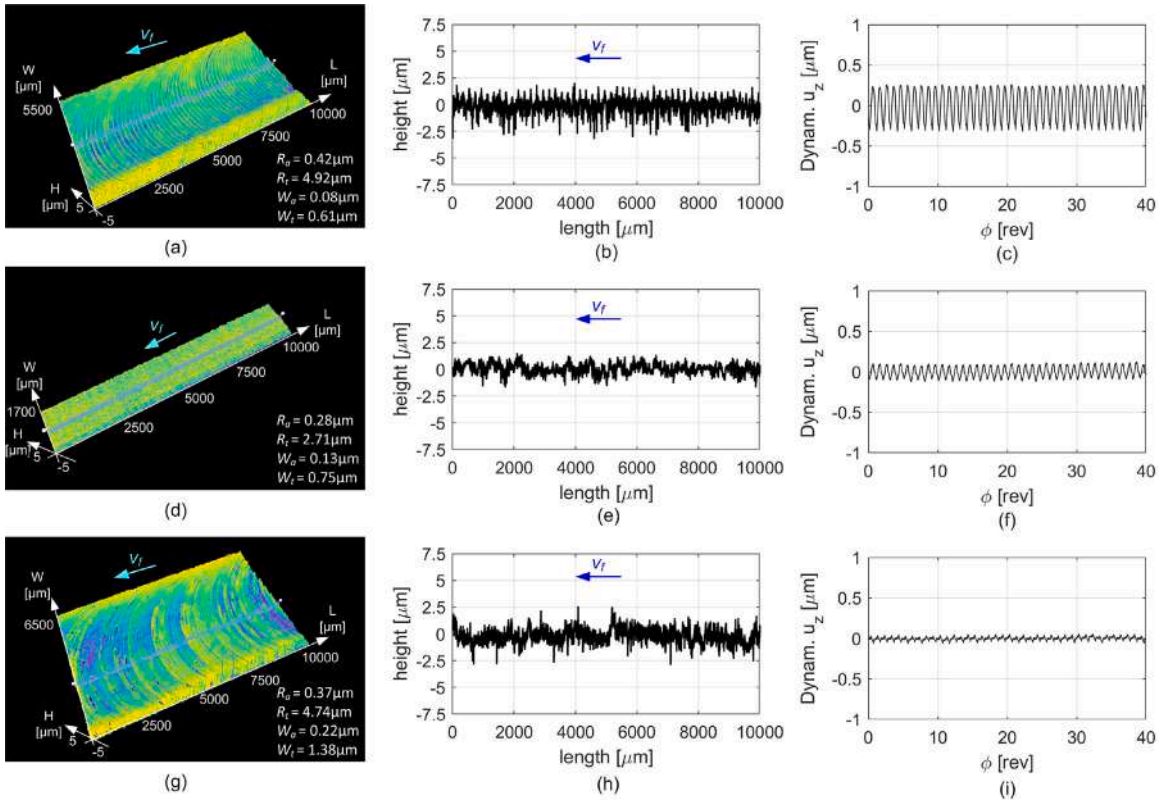

Fig. 14. Machined surface (left), profiles (center) and workpiece axial vibration (right) associated to the cutting test n.1 (top), n.2 (center) and n.3 (bottom) listed in Table 3.

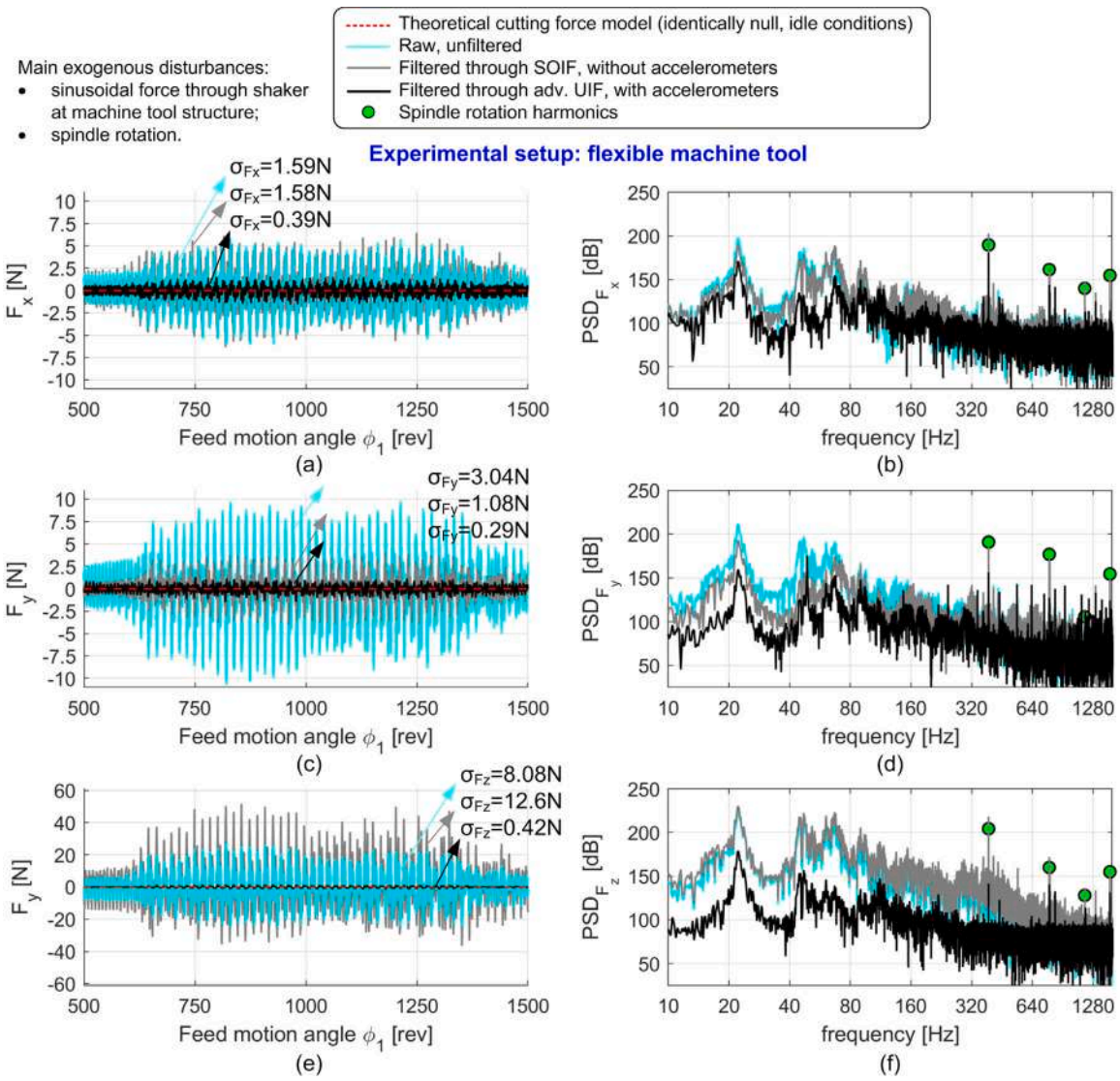

Fig. 15. Analysis in time and frequency domain of the dynamic noise affecting the filtered signals when the spindle is rotating at about $n = 24\,000$ rpm without cutting, at the flexible machine tool (Beckhoff). (For interpretation of the references to color in this figure legend, the reader is referred to the web version of this article.)

the theoretical cutting force model – calibrated under stiff clamping conditions – provided a practical reference for the final cross-validation of the Universal Inverse Filter.

When analyzing the filtered forces derived from the stiff milling machine, no significant differences are visible between the filtered forces illustrated in Figs. 11–13 (except for the differences caused by teeth run-out) and the theoretical forces predicted by the S&P force model, independently from the adopted filter. The main reason for this good behavior is the absence of exogenous noise and the fact that filters have been applied to the same configuration were they have been trained.

The characteristics of the machined surfaces and of the axial vibrations of the workpiece – estimated by the accelerometers attached to the dynamometer base during the cutting process – are given in Fig. 14. In this case, the stiff setup assured a good surface quality in all the considered cases and negligible axial vibrations, as expected.

6.2. Cross-validation of the universal inverse filter at the second milling machine

Afterwards, the performance of the Universal Inverse Filter was assessed at the second, smaller and relatively flexible milling machine.

In this setup even spindle rotation – especially at high rpm – was responsible for significant inertial disturbances affecting the load cells' signals. This is clearly visible in Fig. 15, where the effect of spindle rotation at about 24 000 rpm on the raw and filtered cutting forces is overt. Raw unfiltered force signals (light blue) are significantly disturbed by spindle rotation. When applying the SOIF, the situation is even worsened along the Z direction (gray). An outstanding noise attenuation is achieved both in time and frequency domains only when the novel UIF is applied (black).

A first example of the raw and filtered signals during a real cutting process at the small milling machine is given in Fig. 16. Here an exogenous impulsive force was applied to the machine tool table, just below dynamometer location, in the axial direction. Such disturbance caused an important deviation of the filtered forces with respect to the theoretical trends predicted by the cutting force model. The observed fluctuations may be explained in two ways:

- as inertial disturbances associated to the dynamometer vibrations triggered by the external force;
- as the perturbation of tool-workpiece engagement conditions with respect to the nominal conditions, which can be the consequence of the aforementioned vibrations.

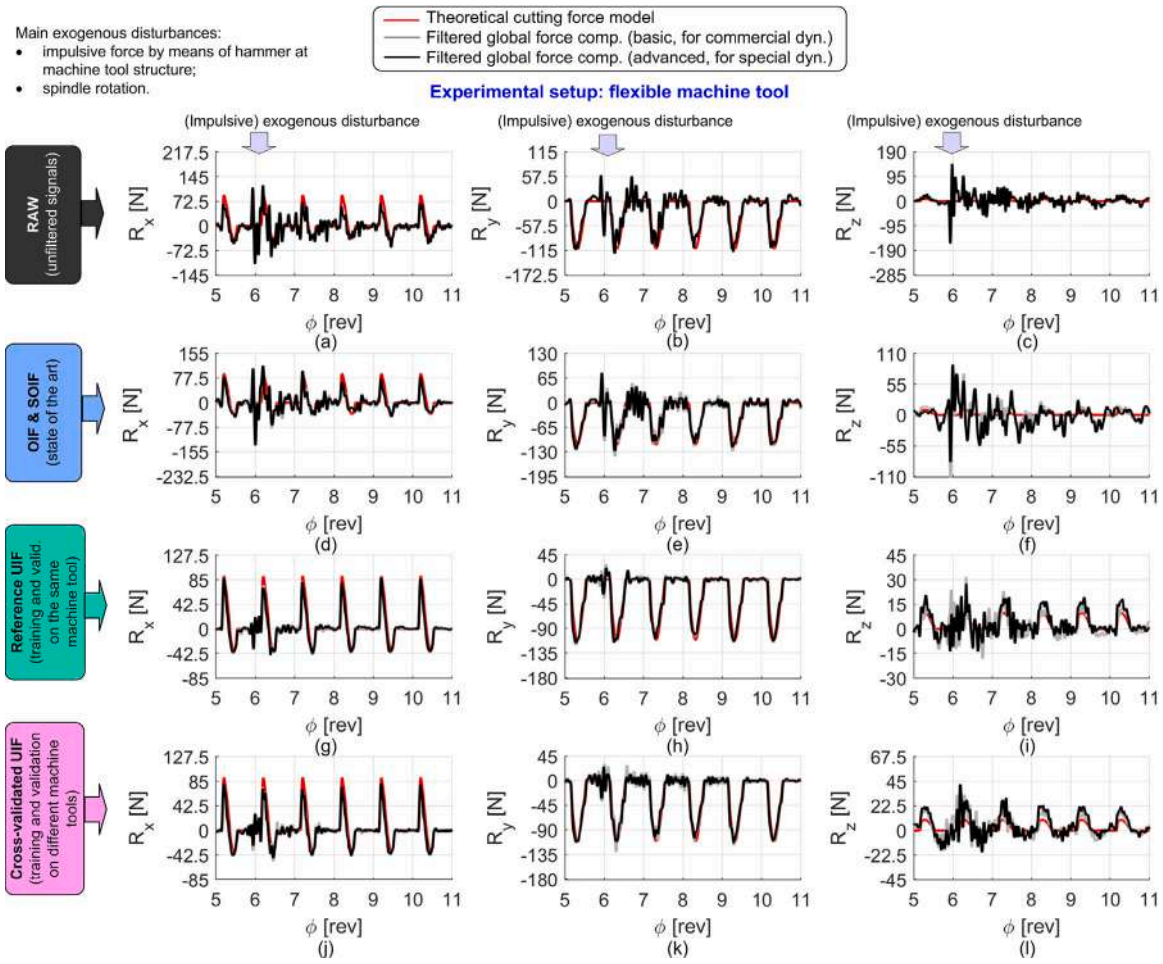

Fig. 16. Comparison between the force components reconstructed from the different filters, under quasi-slotting conditions with the cylindrical endmill at the flexible, small milling machine (Beckhoff). Nominal cutting parameters: $n = 24\,000$ rpm, $f_z = 0.1$ mm, $a_p = 1.2$ mm, $a_{L1} = 2.5$ mm, $a_L = 6.5$ mm.

Table 3
Summary of the selected cutting tests (chosen among the ≈80 tests that have been carried out) illustrated in the figures of this section.

Cutting conditions					Haas			Beck			
Tool	f_z	a_p	$a_{L,1}$, a_L	Test n.	n	Disturb.	Fig.	Test n.	n	Disturb.	Fig.
Cylindrical	0.1	1.2	2.5, 6.5	1			11, 14(a–c)	4		Impulse	16, 20(a–c)
Cylindrical	0.05	1.8	−3.5, 0.5	2	15 000	None	12, 14(d–f)	5	24 000	Sinus.+impulse	17, 20(d–f)
Bull-nose	0.05	1.2	2.5, 6.5	3			13, 14(g–i)	6		Impulse	19, 20(g–i)

The force signals derived from state of the art filters (OIF/SOIF) are the manifestation of the second type of disturbance, or the proof that such filters are unable to compensate purely inertial (exogenous) disturbances?

To answer this question, the machined surface was inspected by a Sensofar S Neox Five Axes 3D confocal microscope featuring a green light source with a wavelength of 530 nm and a Nikon EPI 20x objective, doing a stitching of several fields of view. In addition, vertical vibrations of the workpiece-dynamometer subsystem – expressed in [μm] – were also estimated from the accelerometers located at dynamometer base.

The machined surface is visible in Fig. 20 (a,b), while the axial workpiece vibrations are given in Fig. 20(c). Measurements show that the variations of the axial depth of cut perceived by the active tooth were in the range ±15 μm. Accordingly, the corresponding cutting forces' perturbations should have been moderate. Such perturbations are compatible with the signals processed by UIF whereas they are not compatible with those processed by OIF/SOIF. In summary, the signals derived from the novel UIF are much more realistic than those derived from the state of the art competitors. However, the most important result here is the excellent behavior of the cross-validated UIF, which was trained on the former different setups (stiff milling machine and industrial table), while the reference UIF was trained at the same, small milling machine, for the sake comparison to the best possible filter.

As a second example, a peripheral, down milling operation is illustrated in Fig. 17, which was disturbed by a portable electromagnetic shaker and by the instrumented hammer (acting on the machine tool table, as done before) Raw signals show significant fluctuations (especially along Z direction) plus a localized transient, which are far from the real cutting forces. It is worth recalling that the effective, input cutting forces are identically null when no active teeth are engaged in the workpiece. Contrary to such expectation, both the raw and SOIF version of the axial force component are significantly different than zero almost everywhere. Eventually, the components derived from UIF

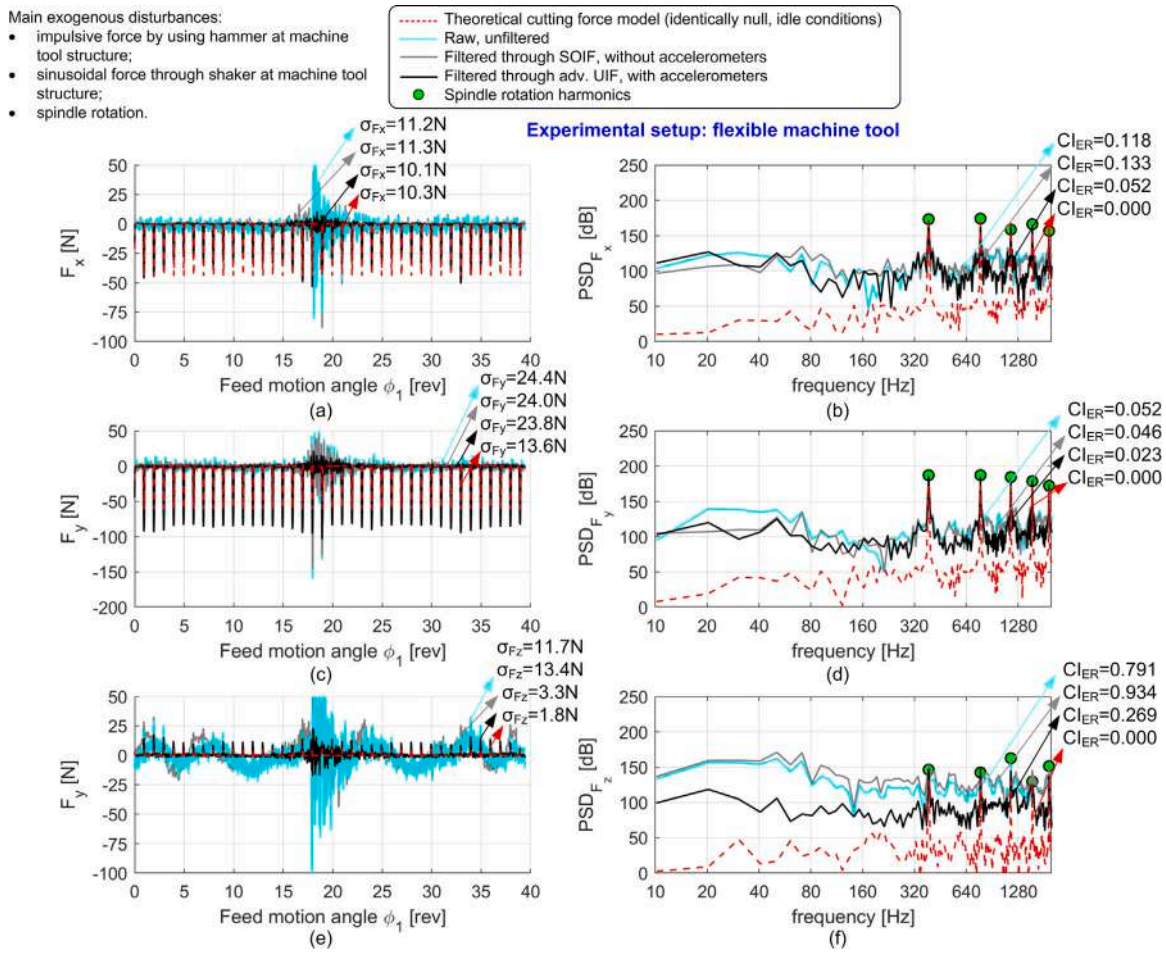

Fig. 17. Analysis in time and frequency domain of the filtered cutting force signals obtained in peripheral down milling with the cylindrical endmill at the flexible machine tool (Beckhoff). Nominal cutting parameters: n = 24 000 rpm, f_z = 0.05 mm, a_p = 1.8 mm, a_{L1} = -3.5 mm, a_L = 0.5 mm.

have a more realistic behavior, which is only slightly modulated and with a smaller degree of instability. This is also confirmed by the measurements of Fig. 20(d–e). Thus, inadequate filtering may influence the classification of process stability, as proved by the radically different values of the classic CI_{ER} indicator associated to the various signals: only those obtained from UIF are realistic.

A further example is given in Fig. 18, where central milling of a thin wall using the cylindrical endmill is reported. Eventually, in Fig. 19 quasi slotting conditions with bull-nose cutter are shown. In all the considered cases, the OIF/SOIF signals are fairly good correlated with the theoretical cutting trends, but the noise caused by spindle rotation and by the external hammer impulse are not well compensated. Again, the moderate variations of the machined surface topographies illustrated in Fig. 20 with respect to the unperturbed conditions are the signature of limited variations of the tool-workpiece engagement conditions. Thus, the force perturbations reconstructed through UIF are closer to the truth than the exaggerated perturbations estimated by state of the art approaches (OIF/SOIF).

In summary, by analyzing the discrepancies between the reconstructed cutting forces and the theoretical, simulated forces, it is clear that OIF/SOIF filters are not capable of compensating both endogenous and exogenous inertial disturbances, which cannot be neglected in the considered cases. In addition, they need to be trained on the same milling machine where they are applied. Their direct application without repeating the identification phase is not possible. On the contrary, the novel UIF method is capable of effectively compensating all the undesired inertial disturbances without the need of repeating the modal analysis and the filter construction phases, which require expert human skills. Such universality is the most important feature of the UIF, while its capability of attenuating all kinds of noise is just a secondary but very welcome property.

From the analysis of all the cutting tests (about 80), the indicators shown in Fig. 21 were obtained. Specifically, the squared linear correlation coefficients R^2_{ii}, where $i = x, y, z$ are given on the left, while the ratio $\sigma_{Ei}/\max|R_i|$ is reported on the right part of the figure. The latter indicator is the standard deviation of the absolute error between model prediction and the filtered force along the ith direction, which was normalized by its maximum absolute value $\max|R_i|$.

On the top part of Fig. 21 the performances of the different algorithms for force reconstruction are reported, when they were applied to the first, stiff milling machine. Under these circumstances, there is no significant difference between UIF and state of the art filters, as expected. In the middle, the key performance indicators obtained at the more flexible and smaller milling machine in the absence of exogenous disturbances – except those deriving from spindle rotation – are given. Here the performance of UIF versus OIF/SOIF is the same along X and Y directions, but considerably better along the Z direction because of the undesired axial vibrations of the workpiece – dynamometer – machine tool table subsystem caused by spindle rotation. Again, it is important to recall that no identification phase was applied on

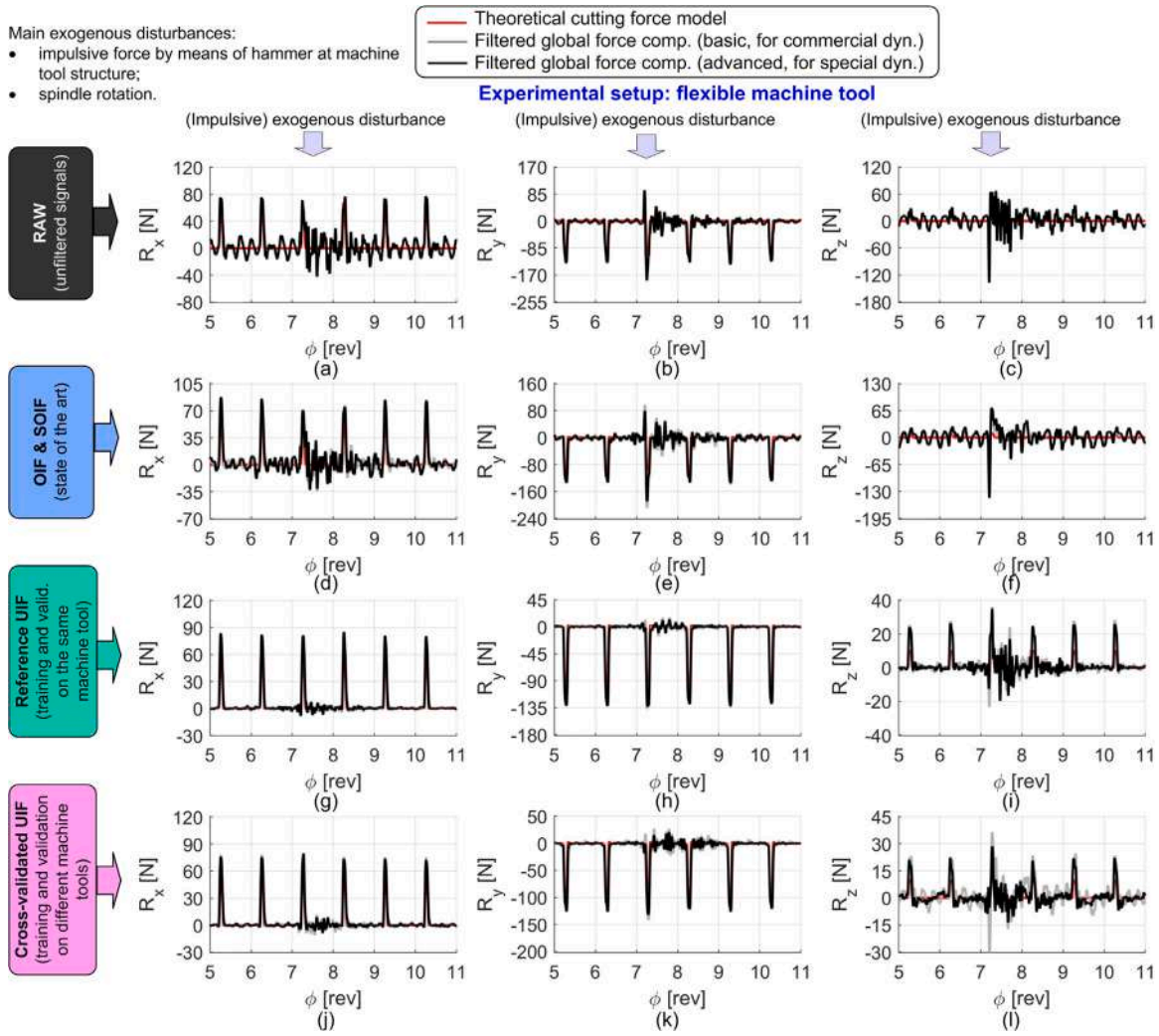

Fig. 18. Comparison between the force components reconstructed from the different filters, under central milling with the cylindrical endmill of a thin walled part at the flexible, small milling machine (Beckhoff). Nominal cutting parameters: $n = 15\,000$ rpm, $f_z = 0.1$ mm, $a_p = 1.2$ mm, $a_{L1} = 1$ mm, $a_L = 2$ mm.

this machine to enable the application of UIF, which is the greatest advantage of this method.

Eventually, in the bottom part of Fig. 21 the key performance indicators derived at the same milling machine but in the presence of additional disturbances (such as the impulsive forces applied to machine tool table) are illustrated. Here the superiority of UIF with respect to OIF/SOIF becomes more apparent along all sensing directions.

Thus, the novel algorithm is capable of achieving an outstanding reconstruction of the effective input cutting forces on any generic machining system without repeating the identification phase, under both noise-free and extremely noisy cutting conditions.

7. Conclusions

In the light of the results obtained in this work we may draw the following conclusions.

All techniques for cutting force reconstruction in milling are based on a preliminary modal analysis phase executed at the machine tool where the dynamometer is mounted. Subsequently, a special algorithm should be launched for computing the filter. These activities are complicated and require skilled human intervention. In addition, cutting force measurements in milling may be affected by exogenous disturbances propagating through the machine tool structure as far as the machine tool table – dynamometer – workpiece subsystem.

In this study, we address the challenges and limitations associated with conventional dynamometers and numerical filters by introducing the Universal Inverse Filter (UIF). To achieve this, a set of accelerometers was integrated into the sensorized fixture, strategically positioned at the base of the dynamometer to capture its six rigid body motions. A preliminary identification phase was conducted under a rigid experimental configuration (where the workpiece was hit) and quasi free–free clamping conditions (where the dynamometer base was hit). Subsequently, the filter was developed through a relatively straightforward regression analysis in the frequency domain. The efficacy of UIF was cross-validated using a distinct experimental setup, specifically a small milling machine. A comparative analysis was performed against potential competitors, namely the Optimal Inverse Filter (OIF) and the Superior Optimal Inverse Filter (SOIF). The non-parametric Upgraded Regularized Deconvolution Filter (URDF) was excluded due to its excessive memory consumption and processing time requirements. Evaluation of the filters' performances was conducted through modal analysis and practical cutting tests carried out on both milling machines.

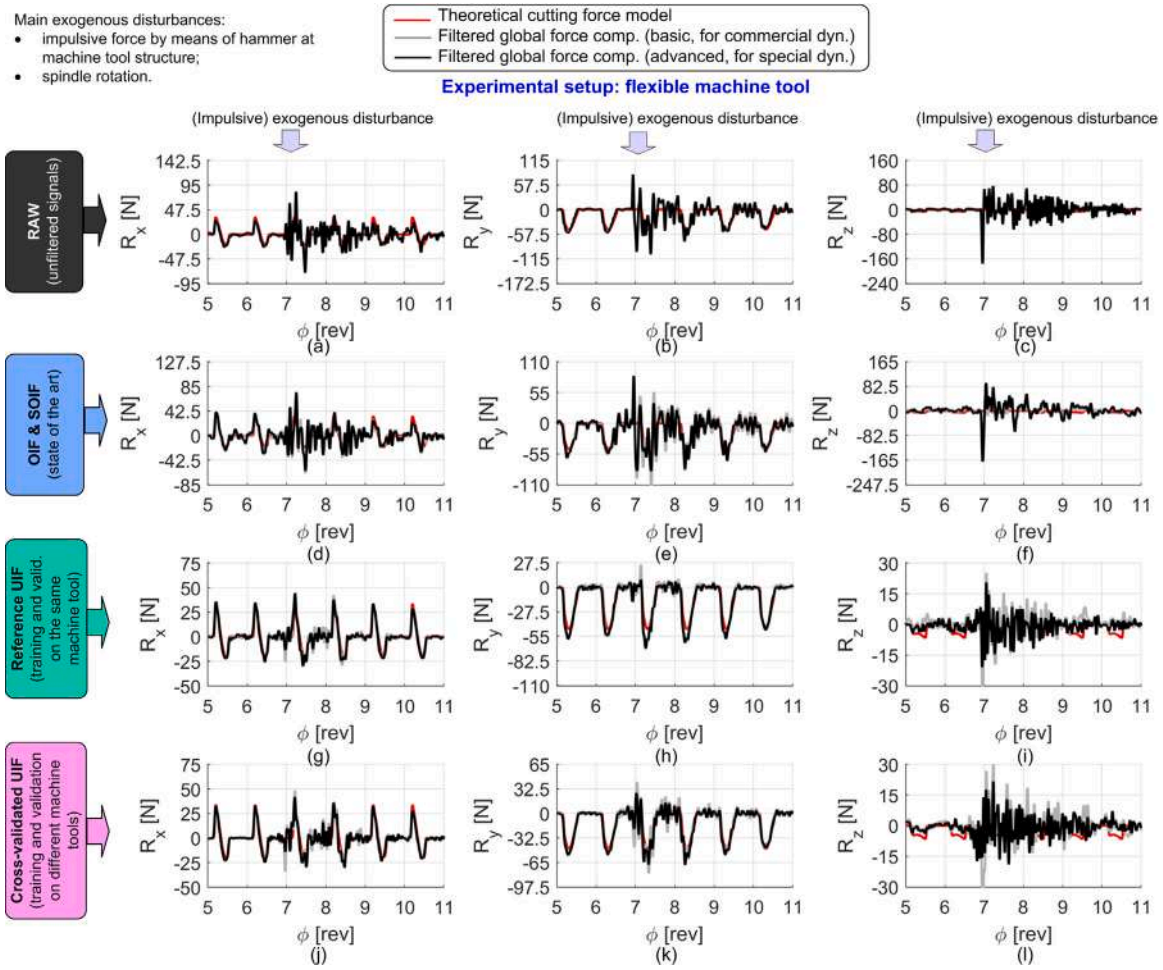

Fig. 19. Comparison between the force components reconstructed from the different filters, under quasi-slotting with the bull-nose cutter (with a single active tooth for avoiding run-out effects) at the flexible, small milling machine (Beckhoff). Nominal cutting parameters: n = 24 000 rpm, f_z = 0.05 mm, a_p = 1.2 mm, a_{L1} = 2.5 mm, a_L = 6.5 mm.

The novel UIF method proved to have similar performances to OIF/SOIF approaches along all direct directions by reaching on average 5 kHz of usable frequency bandwidth. Remarkably, it significantly outperformed the OIF/SOIF along the cross directions (on average 4.5 kHz of compensated bandwidth, more than 4 times better than OIF/SOIF).

Similar conclusions were drawn from the cutting tests conducted on both machine tools where modal analysis was carried out. In essence, UIF showcased its effectiveness without the need for additional calibration on the second, smaller machine tool. The novel filter effectively mitigated both the inertial disturbances arising from the cutting process mechanics and the exogenous disturbances originating from external sources, such as spindle rotation.

The quantitative performance indicators extracted from the cutting tests indicated that the novel approach surpassed state-of-the-art competitors by exhibiting a higher correlation with simulated cutting trends. Additionally, it demonstrated significantly reduced cross-talk, particularly in the presence of exogenous noise, thus corroborating the findings of the modal analysis.

In summary, the experimental validation confirmed the following accomplishments.

- Universality: UIF is truly universal as it is independent of the dynamic behavior of the machine tool where the device is eventually installed. On the contrary, none among the state of the art filters (included OIF, SOIF and URDF) have this important property.
- Comprehensive disturbance attenuation: the novel UIF effectively attenuates all inertial disturbances impacting the load cells' signals, whether endogenous (vibrations caused by cutting forces applied to the workpiece) or exogenous (other vibrational phenomena unrelated to the cutting forces).
- Simplified methodology: the proposed approach significantly simplifies filter calculation compared to the algorithms used for generating other non-parametric state-of-the-art filters such as SOIF and URDF, streamlining unnecessary steps. This property enhances the industrial applicability of the novel filter.
- Versatility: The new approach can be applied to both off-the-shelf and custom-built dynamometers. The addition of accelerometers and execution of a preliminary identification phase, conducted by the device manufacturer or by an expert, enables its use by non-expert technicians across various applications.

Hence, the central concept elucidated herein has the potential to inspire the development of a novel sensing device with numerous promising industrial and commercial applications in machine tools, robotics, and beyond. For instance, the proposed methodology holds promise in robotic milling applications, where it is expected to autonomously address the dependence of dynamometer transmissibility on the robotic arm configuration [37,42]. Consequently, there is a

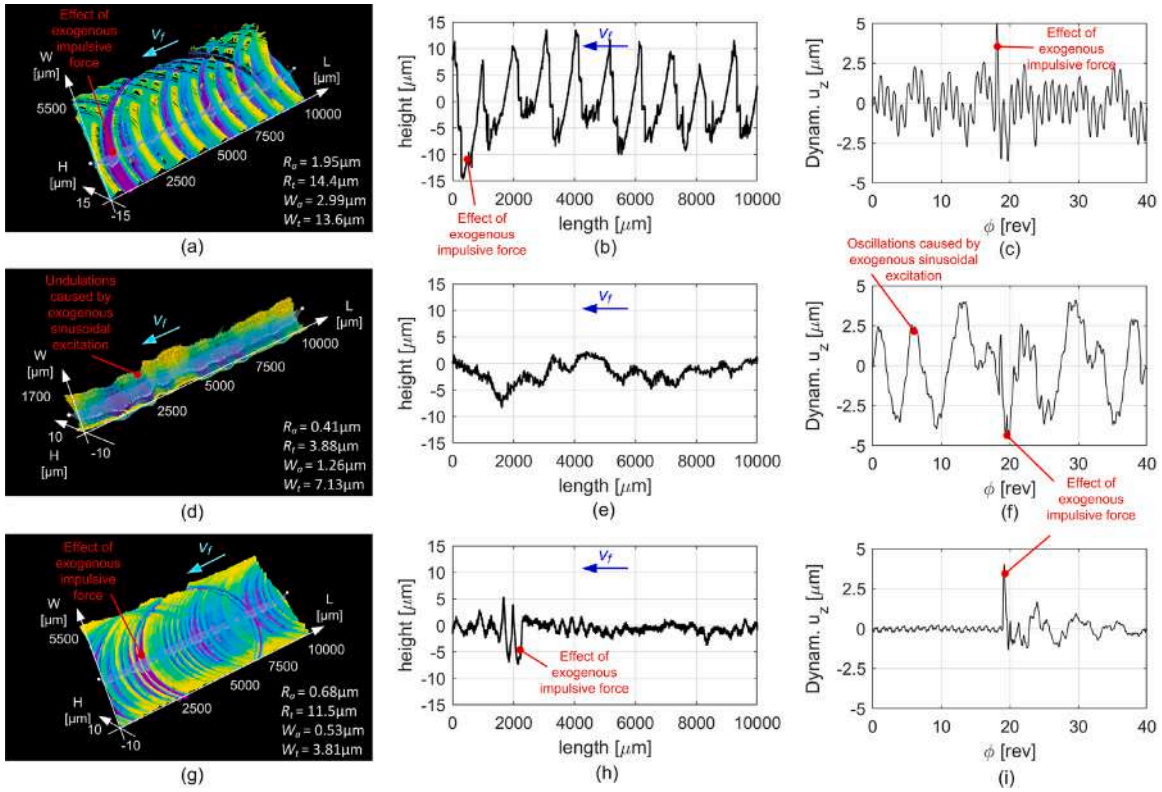

Fig. 20. Machined surface (left), profiles (center) and workpiece axial vibration (right) associated to the cutting test n.4 (top), n.5 (center) and n.6 (bottom) listed in Table 3.

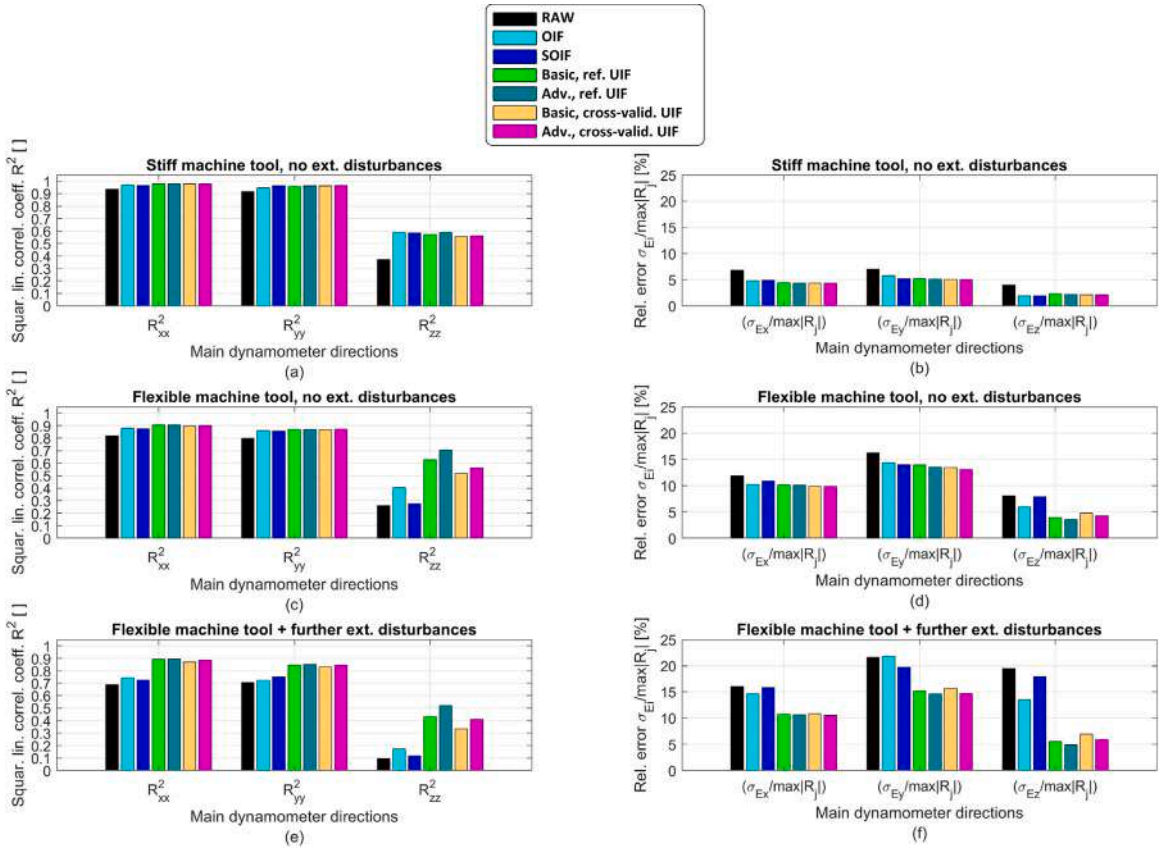

Fig. 21. Final comparison between the novel Universal inverse Filter (UIF) and the state of the art approaches (the Optimal Inverse Filter (OIF) and the Superior Optimal Inverse Filter (SOIF)) derived from cutting tests. On the top (a) and (b) the results obtained at the stiff milling machine; in the middle (c) and (d) the results obtained at the flexible milling machine, without further external disturbances; in the bottom (e) and (f) the results obtained at the flexible milling machine by also introducing some exogenous noise.

keen interest in further exploring this idea within the realm of robotic milling.

CRediT authorship contribution statement

G. Totis: Project administration, Methodology, Investigation, Formal analysis, Data curation, Conceptualization, Software, Validation, Visualization, Writing – original draft. **D. Bortoluzzi:** Investigation, Methodology, Resources, Software, Supervision, Validation, Writing – review & editing. **M. Sortino:** Funding acquisition, Methodology, Resources, Supervision, Validation, Writing – review & editing.

Declaration of competing interest

The authors declare that they have no known competing financial interests or personal relationships that could have appeared to influence the work reported in this paper.

Data availability

Data will be made available on request.

Acknowledgments

The Laboratory for Advanced Mechatronics (LAMA FVG) of the University of Udine is gratefully acknowledged for technical support. LAMA FVG is an international research centre for product and process innovation in which the three Universities of Friuli Venezia Giulia (Italy) cooperate to promote R&D activities at academic and industrial levels.

The authors would also like to thank Beckhoff Automation for the strong support and for the fruitful cooperation to this research activity.

The authors wish to thanking Alessandra Bordon (LAMA FVG) who carried out the measurements with the Sensofar optical instrument.

The authors are particularly grateful to Hexagon AB and AlmaTec S.r.l. for their beneficial cooperation with the University of Udine and their valuable contribution to the creation of LAMA's metrology room.

This study was carried out within the Interconnected Nord-Est Innovation Ecosystem (iNEST) and received funding from the European Union Next Generation EU (PIANO NAZIONALE DI RIPRESA E RESILIENZA (PNRR) – MISSIONE 4 COMPONENTE 2, INVESTIMENTO 1.5 – D.D. 1058 23/06/2022, ECS00000043). This manuscript reflects only the authors' views and opinions, neither the European Union nor the European Commission can be considered responsible for them.

References

[1] G. Bolar, A. Das, S.N. Joshi, Measurement and analysis of cutting force and product surface quality during end-milling of thin-wall components, Measurement 121 (2018) 190–204.

[2] J. Munoa, X. Beudaert, Z. Dombovari, Y. Altintas, E. Budak, C. Brecher, G. Stepan, Chatter suppression techniques in metal cutting, CIRP Ann. Manuf. Technol. 65 (2016) 785–808.

[3] P. Albertelli, M. Goletti, M. Torta, M. Salehi, M. Monno, Model-based broadband estimation of cutting forces and tool vibration in milling through in-process indirect multiple-sensors measurements, Int. J. Adv. Manuf. Technol. 82 (2016) 779–796.

[4] W. Sun, M. Luo, D. Zhang, Machining vibration monitoring based on dynamic clamping force measuring in thin-walled components milling, Int. J. Adv. Manuf. Technol. 1–16 (2020).

[5] K. Ringgaard, Y. Mohammadi, C. Merrild, O. Balling, K. Ahmadi, Optimization of material removal rate in milling of thin-walled structures using penalty cost function, Int. J. Mach. Tools Manuf. 145 (2019) 103430.

[6] Q. Wang, W. Wang, L. Zheng, C. Yun, Force control-based vibration suppression in robotic grinding of large thin-wall shells, Robot. Comput.-Integr. Manuf. 67 (2021) 102031.

[7] C.-P. Wang, K. Erkorkmaz, J. McPhee, S. Engin, In-process digital twin estimation for high-performance machine tools with coupled multibody dynamics, CIRP Ann. Manuf. Technol. 69 (2020) 321–324.

[8] S. Yamato, Y. Kakinuma, Precompensation of machine dynamics for cutting force estimation based on disturbance observer, CIRP Ann. Manuf. Technol. 69 (2020) 333–336.

[9] P. Stavropoulos, H. Bikas, T. Souflas, M. Ghassempouri, A method for cutting force estimation through joint current signals in robotic machining, Procedia Manuf. 55 (2021) 124–131.

[10] J. Chae, S.S. Park, High frequency bandwidth measurements of micro cutting forces, Int. J. Mach. Tools Manuf. 47 (2007) 1433–1441.

[11] E. Korkmaz, B. Bediz, B.A. Gozen, O.B. Ozdoganlar, Dynamic characterization of multi-axis dynamometers, Precis. Eng. 38 (2014) 148–161.

[12] G. Totis, M. Sortino, Upgraded regularized deconvolution of complex dynamometer dynamics for an improved correction of cutting forces in milling, Mech. Syst. Signal Process. 166 (2022) 108412.

[13] G. Totis, O. Adams, M. Sortino, D. Veselovac, F. Klocke, Development of an innovative plate dynamometer for advanced milling and drilling applications, Measurement 49 (2014) 164–181.

[14] G. Totis, M. Sortino, Superior optimal inverse filtering of cutting forces in milling of thin-walled components, Measurement 206 (2023) 112227.

[15] G. Totis, G. Wirtz, M. Sortino, D. Veselovac, E. Kuljanic, F. Klocke, Development of a dynamometer for measuring individual cutting edge forces in face milling, Mech. Syst. Signal Process. 24 (2010) 1844–1857.

[16] M. Rizal, J. Ghani, M. Nuawi, C. Hassan, C. Haron, Development and testing of an integrated rotating dynamometer on tool holder for milling process, Mech. Syst. Signal Process. 52–53 (2015) 559–576.

[17] Z. Xie, Y. Lu, J. Li, Development and testing of an integrated smart tool holder for four-component cutting force measurement, Mech. Syst. Signal Process. 93 (2017) 225–240.

[18] M. Luo, H. Luo, D. Axinte, D. Liu, J. Mei, Z. Liao, A wireless instrumented milling cutter system with embedded PVDF sensors, Mech. Syst. Signal Process. 110 (2018) 556–568.

[19] V. Nguyen, J. Johnson, S. Melkote, Active vibration suppression in robotic milling using optimal control, Int. J. Mach. Tools Manuf. 152 (2020) 103541.

[20] A. Albrecht, S.S. Park, Y. Altintas, G. Pritschow, High frequency bandwidth cutting force measurement in milling using capacitance displacement sensors, Int. J. Mach. Tools Manuf. 45 (2005) 993–1008.

[21] G. Totis, Z. Dombovari, M. Sortino, Upgraded Kalman filtering of cutting forces in milling, Sensors 20 (2020) 5397.

[22] B. Qiao, X. Zhang, J. Gao, R. Liu, X. Chen, Sparse deconvolution for the large-scale ill-posed inverse problem of impact force reconstruction, Mech. Syst. Signal Process. 83 (2017) 93–115.

[23] C. Pan, X. Ye, J. Zhou, Z. Sun, Matrix regularization-based method for large-scale inverse problem of force identification, Mech. Syst. Signal Process. 140 (2020) 106698.

[24] A. Jullien-Corrigan, K. Ahmadi, Measurement of high-frequency milling forces using piezoelectric dynamometers with dynamic compensation, Precis. Eng. 66 (2020) 1–9.

[25] B. Qiao, Z. Mao, J. Liu, Z. Zhao, X. Chen, Group sparse regularization for impact force identification in time domain, J. Sound Vib. 445 (2019) 44–63.

[26] B. Qiao, C. Ao, Z. Mao, X. Chen, Non-convex sparse regularization for impact force identification, J. Sound Vib. 477 (2020) 115311.

[27] L.R. Castro, P. Vieville, P. Lipinski, Correction of dynamic effects on force measurements made with piezoelectric dynamometers, Int. J. Mach. Tools Manuf. 46 (2016) 1707–1715.

[28] F. Girardin, D. Remond, J.F. Rigal, High frequency correction of dynamometer for cutting force observation in milling, J. Manuf. Sci. Eng. 132/031002 (2010).

[29] M. Wan, W. Yin, W.-H. Zhang, H. Liu, Improved inverse filter for the correction of distorted measured cutting forces, Int. J. Mech. Sci. 120 (2017) 276–285.

[30] E. Korkmaz, B.A. Gozen, B. Bediz, O.B. Ozdoganlar, Accurate measurement of micromachining forces through dynamic compensation of dynamometers, Precis. Eng. 49 (2017) 365–376.

[31] S.A. Spiewak, Acceleration based indirect force measurement in metal cutting processes, Int. J. Mach. Tools & Manuf. 35/1 (1995) 1–17.

[32] N. Tounsi, A. Otho, Dynamic cutting force measuring, Int. J. Mach. Tools Manuf. 40 (2000) 1157–1170.

[33] H. Mostaghimi, C.I. Park, G. Kang, S.S. Park, D.Y. Lee, Reconstruction of cutting forces through fusion of accelerometer and spindle current signals, J. Manuf. Process. 68 (2021) 990–1003.

[34] M. Postel, D. Aslan, K. Wegener, Y. Altintas, Monitoring of vibrations and cutting forces with spindle mounted vibration sensors, CIRP Ann. Manuf. Technol. 68 (2019) 413–416.

[35] K. Takahei, N. Suzuki, E. Shamoto, Identification of the model parameter for milling process simulation with sensor-integrated disturbance observer, Precis. Eng. 78 (2022) 146–162.

[36] C.H. Mun, S. Rezvani, J. Lee, S.S. Park, H.W. Park, J. Lee, Indirect measurement of cutting forces during robotic milling using multiple sensors and a machine learning-based system identifier, J. Manuf. Process. 85 (2023) 963–976.

[37] C. Oh, J.H. Lee, T.I. Ha, B.K. Min, Model parameter identification of a machining robot using joint frequency response functions, Int. J. Precis. Eng. Manuf. 24 (2023) 1647–1659.

[38] M. Joddar, K. Ahmadi, Estimating milling forces from vibration measurements, in: Proceedings of ASME 2022 17th International Manufacturing Science and Engineering Conference, MSEC2022-85157, V001T04A001.

[39] C. Wang, X. Zhang, B. Qiao, H. Cao, Xuefeng ChenDynamic force identification in peripheral milling based on CGLS using filtered acceleration signals and averaged transfer functions, J. Manuf. Sci. Eng. 141 (6) (2019) 064501.

[40] M. Wan, W.-J. Pan, W.-H. Zhang, Y.-C. Ma, Y. Yang, A unified instantaneous cutting force model for flat end mills with variable geometries, J. Mater Process. Technol. 214 (2014) 641–650.

[41] G. Totis, Breakthrough of regenerative chatter modeling in milling by including unexpected effects arising from tooling system deflection, Int. J. Adv. Manuf. Technol. 89 (2017) 2515–2534.

[42] S. Xin, F. Peng, X. Tang, R. Yan, Z. Li, J. Wu, Research on the influence of robot structural mode on regenerative chatter in milling and analysis of stability boundary improvement domain, Int. J. Mach. Tools Manuf. 179 (2022) 103918.